

Numerical analysis of contact electrification of non-spherical particles in a rotating drum

Pei, Chunlei; Wu, Chuan-yu; Adams, Michael

DOI:

[10.1016/j.powtec.2015.05.050](https://doi.org/10.1016/j.powtec.2015.05.050)

License:

Creative Commons: Attribution-NonCommercial-NoDerivs (CC BY-NC-ND)

Document Version

Peer reviewed version

Citation for published version (Harvard):

Pei, C, Wu, C & Adams, M 2015, 'Numerical analysis of contact electrification of non-spherical particles in a rotating drum', *Powder Technology*, vol. 285, pp. 110-122. <https://doi.org/10.1016/j.powtec.2015.05.050>

[Link to publication on Research at Birmingham portal](#)

Publisher Rights Statement:

Eligibility for repository: checked 07/10/2015

General rights

Unless a licence is specified above, all rights (including copyright and moral rights) in this document are retained by the authors and/or the copyright holders. The express permission of the copyright holder must be obtained for any use of this material other than for purposes permitted by law.

- Users may freely distribute the URL that is used to identify this publication.
- Users may download and/or print one copy of the publication from the University of Birmingham research portal for the purpose of private study or non-commercial research.
- User may use extracts from the document in line with the concept of 'fair dealing' under the Copyright, Designs and Patents Act 1988 (?)
- Users may not further distribute the material nor use it for the purposes of commercial gain.

Where a licence is displayed above, please note the terms and conditions of the licence govern your use of this document.

When citing, please reference the published version.

Take down policy

While the University of Birmingham exercises care and attention in making items available there are rare occasions when an item has been uploaded in error or has been deemed to be commercially or otherwise sensitive.

If you believe that this is the case for this document, please contact UBIRA@lists.bham.ac.uk providing details and we will remove access to the work immediately and investigate.

Accepted Manuscript

Numerical Analysis of Contact Electrification of Non-spherical Particles in a Rotating Drum

Chunlei Pei, Chuan-Yu Wu, Michael Adams

PII: S0032-5910(15)00479-9
DOI: doi: [10.1016/j.powtec.2015.05.050](https://doi.org/10.1016/j.powtec.2015.05.050)
Reference: PTEC 11064

To appear in: *Powder Technology*



Please cite this article as: Chunlei Pei, Chuan-Yu Wu, Michael Adams, Numerical Analysis of Contact Electrification of Non-spherical Particles in a Rotating Drum, *Powder Technology* (2015), doi: [10.1016/j.powtec.2015.05.050](https://doi.org/10.1016/j.powtec.2015.05.050)

This is a PDF file of an unedited manuscript that has been accepted for publication. As a service to our customers we are providing this early version of the manuscript. The manuscript will undergo copyediting, typesetting, and review of the resulting proof before it is published in its final form. Please note that during the production process errors may be discovered which could affect the content, and all legal disclaimers that apply to the journal pertain.

Numerical Analysis of Contact Electrification of Non-spherical Particles in a Rotating Drum

Chunlei Pei^{1,2,ζ}, Chuan-Yu Wu^{1*}, Michael Adams²

¹ Department of Chemical and Process Engineering, University of Surrey, Guildford, Surrey, GU2 7XH, UK

² School of Chemical Engineering, University of Birmingham, Birmingham, B15 2TT, UK

Abstract

Contact electrification is generally referred to as the charge transfer process between particles during collisions. The transferred charge can be accumulated on the surface of the particles especially for insulating materials with irregular shapes, which can lead to a non-uniform charge distribution and eventually affects the charge accumulation process. In this study, in order to investigate the influence of the particle shape on contact electrification, a sphere-tree multi-sphere method and a contact electrification model are implemented into the discrete element method (DEM) to model the charging process of irregular particles in a rotating drum. Irregular particles with various Sauter mean diameters but the same maximum diameter and equivalent volume diameters are considered. The charge distribution and accumulation on the particles are investigated. It is found that the charge transfer originates from the contact between the particle and the drum due to the contact potential difference and

^ζ Presently with Department of Materials Science and Metallurgy, University of Cambridge, Cambridge, CB3 0FS, UK

* Corresponding author: Tel: 01483683506. Email: c.y.wu@surrey.ac.uk

initially takes place primarily at the region near the wall of the drum. The charge eventually propagates to the entire granular bed. The charge of the particles increases exponentially to an equilibrium value. For particles with the same maximum diameter, a larger charging coefficient is obtained for the particles with smaller Sauter mean diameters and sphericities, which lead to a faster charge accumulation, while for particles with the same equivalent volume diameter and fill ratio, similar charging coefficients are observed. A non-uniform intra-particle charge distribution is induced on each individual multi-sphere particle.

Keyword: contact electrification; particle shape; discrete element method; charge distribution.

1. Introduction

Contact electrification is generally referred to as a charge transfer process between objects during collisions [1,2]. It occurs commonly in powder handling processes where particles can have intensive mechanical contacts. During the contact, electrostatic charges migrate from one surface to another and accumulate on the particles. The transferred charges can be retained on particle surfaces especially for insulating materials [3,4], which can lead to a non-uniform charge distribution and eventually affect the charge accumulation process. The accumulated charges on particle surfaces will induce electrostatic interactions that can significantly influence the dynamic behaviours of particles, especially when the electrostatic forces become dominant over the gravitation of particles [5]. It can cause segregation [6], agglomeration [7–9], suspension [10] and even explosion [11] within the particle system. These phenomena are usually detrimental and can extremely diminish the performance of powder handling processes. Therefore, the investigation of the charge transfer and

accumulation is of the fundamental importance to minimize the electrostatic effects and improve the performance of powder handling processes.

The charge acquisition and distribution within the particle system, which are also called inter-particle charge acquisition and distribution, were investigated experimentally and numerically [2,12–14]. LaMarche et al. [12] examined the charging process of dielectric particles flowing through a metal cylinder and showed that the net charge on the particles increased linearly with an increase in the contact surface area between the particles and the cylinder, while the net charge density of the powder was greater in the region close to the wall compared with that at the centre. They attributed that the charge acquisition of the powder initially occurs primarily during the contact between the particles and the cylinder. However, it is extremely difficult to obtain detailed information from each particle in the dynamic system experimentally [15–17]. Therefore, the discrete element method coupled with computational fluid dynamics (DEM-CFD) has been widely used to explore the physical and mechanical behaviours of each individual particle and subsequent bulk properties of the particle system. Pei et al. [13] used the DEM-CFD implemented with a contact electrification (condenser) model to compute the charging process of particles in a fluidized bed. It was found that the electrostatic charge was initially generated after the impact between the particle and the container surfaces at side regions close to container surfaces due to different work functions between particles and container surfaces. Then the charge propagated from the side regions to the central region of the granular bed. Eventually, the charge of the particle system reached an equilibrium state. These phenomena were consistent with the experimental observations of LaMarche et al. [12] and Guardiola *et al.* [14].

The charging process becomes more complicated when particles of irregular shapes are used in powder handling process [18–22]. Yao et al. [18,19] investigated the effect of the particle shape on the charging process when the particle is sliding on the surface of a stainless steel pipe. In their study, the polyvinyl chloride (PVC) granules were made into triangular and trapezoidal shapes. Due to the shape difference, particles with larger sliding (contact) area obtained higher electrostatic charge. They also suggested that the particle orientation influenced the sliding velocity. The particles with an orientation which can induce a larger sliding velocity acquired high charge in the process. For insulating materials, the electrostatic charge can concentrate on the contact area and lead to an intra-particle charge distribution on the surface of each particle. Ireland [21] modelled the charge transfer between a 2-D elliptic particle and a tilted surface during impact using DEM. The surface of each particle was divided into segments and the charge was only transferred onto the segments inside the contact area because of the insulating nature of the particle. It was shown that for the contact electrification of an elliptic particle impacting (bouncing) on a surface, the particle with a lower roundness ratio (defined as the ratio of radii between the major axis and the minor axis) led to a larger contact area. In addition, the transferred charge was larger with a larger contact area, which meant that the contact and charge transfer process could be affected by particle shape. Pei et al. [20] investigated the intra-particle charge distribution of elongated particles in a vibrating container. Using the symmetric multi-sphere method [23], the elongated particle was approximated by a row of axisymmetric primary spheres with various sizes. Due to the shape effect, the elongated particles tend to be orthogonal to the vibrating direction and parallel to the top and bottom surfaces, which causes that the larger primary spheres have higher contact rates with container surfaces and other particles and consequently obtain higher charges especially at the early vibrating stage. In other words, for convex elongated particles, the central part of the particle was larger and easier to make contact with the

container surface and acquired charge, while for concave elongated particles, the distal part of the particle was larger and more vulnerable to get charged during the vibration. This reveals that the particle shape can cause non-uniform intra-particle charge distribution and consequently different charging behaviours. Matsuyama *et al.* [22] suggested that the induced potential difference was mainly induced by the local transferred charge at the contact area while the charge at the remote (rear) side to the contact area had less effect on the induced potential difference. Therefore, the particle shape can affect inter-and intra-particle charge distribution and accumulation. However, the study on these effects is still inadequate especially for more complex shapes and various powder handling processes.

In this paper, charge distribution and accumulation of irregular particles in a rotating drum is analysed using DEM implemented with a contact electrification model. A multi-sphere method is used to approximate the particle shape that is illustrated in the next section. The particle profiles and charging process in the rotating drum are presented and discussed. In addition, the intra-particle charge distribution is also examined.

2. Methodology

2.1 The multi-sphere DEM model

In practical powder handling processes, the shape of the particle is usually non-spherical and irregular. The irregular particle shape can lead to various dynamic behaviours and alter the charging process during powder handling processes. In the current study, to investigate the effect of the particle shape on contact electrification, the particle shape is approximated using a sphere-tree multi-sphere method [24,25]. For instance, the geometry of the particle can be

represented by a 3D object. Then the surface of the particle is meshed into triangular elements and the particle is represented using a polyhedron (Figure 1). The sphere-tree construction toolkit (<http://isg.cs.tcd.ie/spheretree/>) developed by Bradshaw and O'Sullivan [25] is then used to construct the particle (multi-sphere) with a selection of primary spheres of various sizes to approximate the shape of the meshed particle.

The medial axis approximation method is used to generate the multi-sphere assembled by primary spheres [25]. First, the surface of the polyhedron is sampled with a number of seeds as shown in Figure 1. Secondly a Voronoi diagram with connected cells is constructed so that each Voronoi cell represents the region of space that is closer to its corresponding seed than any other seeds. Then primary spheres can then be generated within cells and scaled to fit the surface with optimised coverage, e.g. the smallest distance between the seeds and the surfaces of the primary spheres, as shown in Figure 2.

A merge optimization method can also be used to control and reduce the number of primary spheres [25]. In this method, each pair of neighbouring spheres are merged and approximated by a new parent sphere that should contain the same set of surface seeds covered by the child neighbouring pair. This method can be iterated until the desired number of primary spheres is reached as illustrated in Figure 3. This method is particularly useful for generating a small number of primary spheres that can be implemented into DEM simulations to save computational time. However, the accuracy for the geometric approximation of this method depends on the number of the primary spheres which can be seen by comparing Figure 2 with Figure 3. The relative error between the volumes of the multi-sphere and the polyhedron can vary in a large range (e.g. 20% - 200%), depending on the approximation method and number of primary spheres [26].

Due to the complex construction of primary spheres for a particle, it is difficult to determine the mass properties of the particles based on the multi-sphere model. As a first approximation, the mass properties of the particle can be calculated using the integral method [27] with respect to triangular elements of the polyhedron. This integral method can be further reduced to three steps: line integral, projection integral and surface integral. The approach (<http://www.cs.berkeley.edu/~jfc/mirtich/massProps.html>) developed by Mirtich [27] is used to calculate the mass properties of the polyhedron (particle), i.e. the location of the mass centre, the volume, and the inertia properties (principle moments of inertia and principle axes of inertia).

Once the multi-sphere is constructed, each particle is imported into the DEM for further analysis. The connection (overlap) between primary spheres is considered as rigid. The contact detection is based on primary spheres. Contact forces and moments between primary spheres within different particles are calculated once the contacts between these primary spheres are determined. For elastic particles, the normal contact is modelled using Hertz theory [28], and that of Mindlin and Deresiewicz [29] is employed for the tangential interaction. The contact forces and moments are then integrated on the mass centre of the each particle in contact [23]. The dynamics of the irregular particles is calculated by Newton's second law of motion.

2.2. The contact electrification model

Contact electrification process is referred to as the charge transfer between surfaces due to the potential difference during contacts. The transferred charge can induce electric field and

further polarization of the charge distribution on the particle surface. These effects play important roles in the charge transfer process. The contact electrification model in this DEM model is based on the primary sphere, which is similar to the model reported in Pei et al. [13,20]. When a contact occurs, the charge can be transferred from one surface to another due to the total potential difference which can be expressed as:

$$\Delta V = V_c - V' = V_i - V_j - V' \quad (1)$$

where ΔV is the total potential difference; $V_c (=V_i - V_j)$ is the contact potential difference (CPD) between the surfaces; V' is the induced potential difference; V_i and V_j are the work function potential of material i and j , respectively.

The induced potential difference is caused by the electric field between two charged objects and related to the local charge density distribution on surfaces of charged objects [22]. As shown in Figures 2 and 3, the overlaps between primary spheres are significant. A large portion of the surface of the primary sphere is buried inside the volume of the particle and does not contribute to the actual surface of the particle, which is different from the axisymmetric multi-sphere method [20]. Therefore, the induced potential between the wall surface and the charged primary sphere at the contact area is given as follows:

$$V' = k_0 q_s = \xi \frac{z}{\epsilon_0} A_{sp}^{-1} q_s \quad (2a)$$

$$k_0 = \xi \frac{z}{\epsilon_0} A_{sp}^{-1} \quad (2b)$$

where A_{sp} is the equivalent surface area of the primary sphere; q_s is the charge of the particle; ϵ_0 is the permittivity of a vacuum (8.854×10^{-12} F·m⁻¹), z is the contact gap for tunnel relaxation of the order of a few nano-meters to hundreds of nano-meters [30], which is 130 nm in the current study; ξ is the image correction factor due to the polarization effects. The induced electric field can further polarize the surface and cause the image effects. If the image effects are considered, the induced potential difference can be affected by the image correction factor, depending on the dielectric properties and the contact gap (e.g. in range of 1 – 10) [31]. In the current study, the wall surface is assumed to be conductive, so this image correction factor is set to 2 [2,31]. It should be noted that, according to Eqs. (1) and (2), the CPD will be eventually balanced by the induced potential difference that is determined by the charge of particles and the induced image effects. Therefore, the image correction factor can influence the final equilibrium charge on the particle. For instance, assuming that the CPD is constant, the final equilibrium charge decreases with the increase of the image correction factor. In other words, the dielectric properties and contact conditions can play important role in the charging transfer process.

If two charged primary spheres of insulating materials are considered, then the induced potential difference can be determined as:

$$V' = \frac{z}{\epsilon_0} \left(\frac{q_{sj}}{A_{spj}} - \frac{q_{si}}{A_{spi}} \right) \quad (2c)$$

where q_{si} and q_{sj} are the charge of primary spheres i and j ; A_{spi} and A_{spj} are the equivalent surface areas of the primary spheres i and j , which can be defined as:

$$A_{sp} = \frac{A_p}{n_p} \quad (3)$$

where A_p is the surface area of the particle; n_p is the number of the primary spheres; A_{sp} is the equivalent area which is the mean division of the particle surface area by the number of primary spheres. It can be seen that the charge transfer depends on the local polarization of the particle, which is similar to the contact electrification model for the axisymmetric multi-sphere method [20]. In the current study, primary spheres are assumed to be perfect insulators so the charge does not relax and redistribute between primary spheres. The contact gap between spheres, z is equal to 260 nm and the image effects between particles are ignored. The charge on particles (space charge) can induce electric field in the space, which will lead to electrostatic interactions between charged objects during the process. This electric field may further alter the charge transfer process. As relative large and insulating particles are used in the current study, the electrostatic interactions between objects are ignored, and consequently, the effect of space charge are also not considered.

Based on the condenser model [2,13,32], the CPD ($V_c = V_i - V_j$) is the driving force for electron transfer between contacting surfaces. In each collision, the transferred charge is proportional to the maximum contact area and the total potential difference:

$$\Delta q = k_s S_m \Delta V \quad (4)$$

where S_m is the maximum contact area during the collision, k_s is the charging constant during contact electrification and is of the order of $10^{-4} \text{ C} \cdot \text{m}^{-2} \cdot \text{V}^{-1}$ [32–34]. During a collision, the

charge will be transferred from material i to material j . Hence after each collision, the charge on these materials will become $q_{si}-\Delta q$ and $q_{sj}+\Delta q$, respectively.

2.3. The model setup

The contact electrification process of particles with arbitrary shapes in a rotating drum is modelled using the developed DEM with the contact electrification model. The model setup is shown in Figure 4. The cylindrical drum with a 3 mm diameter and 5 mm length is discretized into 504 triangular meshes. The contact interactions are detected and applied between particles and each triangular mesh [35]. Initially, 300 (multi-sphere) particles are deposited on the cylindrical surface of the drum until the granular bed is stable (i.e. the maximum particle velocity is smaller than 10^{-6} m·s⁻¹). Then the drum will start to rotate around the x axis at 30 rpm. The contact electrification model will be applied once the drum starts to rotate.

To investigate the effects of particle shape, 4 types of multi-spheres are used in the DEM simulations. The particles represented by polyhedrons are shown in Figure 5. Particle I, II, III and IV consist of 440, 744, 266, 544 triangular meshes, respectively. Then the corresponding multi-sphere to each particle is generated using the medial axis approximation as illustrated in Figure 5. Each particle is constructed with 8 primary spheres, respectively. Spherical particles (Particle V) are also used for reference and comparison.

In order to characterize the particle size and shape, several particle parameters, including maximum diameter, Sauter mean diameter, equivalent volume diameter, and sphericity, are used to classify irregular particles.

The maximum diameter of the particle, D_{max} , is defined as the largest distance between two vertices of the polyhedral particle. The surface area is determined as the summation of the areas of all triangular meshes. The volume of each particle is calculated using the integral method [27].

The Sauter mean diameter (SMD) of the particle is defined as [36]:

$$D_{32} = 6 \frac{\psi_p}{A_p} \quad (5)$$

where ψ_p is the volume of the polyhedron (particle); A_p is the surface area of the polyhedron (particle). From Eq. (5), it can be seen that D_{32} is related to the surface-to-volume ratio and is defined as the ratio between the surface area and the volume of the particle. For the same maximum diameter, a smaller value of D_{32} results in a larger surface-to-volume ratio, which means larger active surface per unit volume.

The shape of the particles are classified using the dimensionless sphericity of the particles [37] defined as:

$$\zeta = \frac{\pi^{1/3} (6\psi_p)^{2/3}}{A_p} \quad (6)$$

From Eqs. (5) and (6), it can be seen that, for the same maximum diameter, a larger value of D_{32} will lead to a higher sphericity. The sphericity of the spherical particles is 1.0.

The equivalent volume diameter, D_v , is defined as [38]:

$$D_v = \left(\frac{6}{\pi} \psi_p \right)^{1/3} \quad (7)$$

It can be seen that equivalent volume diameter is the diameter of the sphere with the same volume as the irregular particle.

In this study, particles with the same D_{max} and D_v are used as shown in Tables 1 and 2. Particles with the same D_{max} but different shapes (D_{32} and sphericity) can have different fill ratio that is the volume ratio between particles and the drum. For particles with the same D_{max} , the influence of various particle shapes and fill ratio on the charge distribution and accumulation are analysed and discussed (see Results section). Particles with the same D_v and fill ratio are also used for comparison, especially for the charge accumulation process (see Discussions section). The physical properties of the particle and the drum are the same as those given in Table 3. The work functions of the particles and the drum are 4.52 and 4.7 V, respectively. When the drum starts to rotate, the charge will be transferred between the particles and between the particle and the drum. In reality, the charge accumulation on particles takes much more time to reach saturation, which is extremely computationally expensive for DEM simulations. Consequently, the charging constant k_s is set to $0.02 \text{ C} \cdot \text{m}^{-2} \cdot \text{V}^{-1}$ in order to accelerate the charging process in the DEM simulations. The charge is assumed to be attained by the primary sphere and is not re-distributed onto other primary spheres and dissipated to the environment. In addition, the electrostatic interactions are also ignored in this study.

3. Results

3.1. The particle profiles

Figure 6 shows the perspective view of particle I ($D_{32} = 3.72 \times 10^{-4}$ m) profiles during the drum rotation from the x direction. Initially (Figure 6a), the particles lay on the cylindrical surface of the drum. When the drum starts to rotate, the granular bed follows the movement of the cylindrical surface of the drum and forms an inclination angle with the x - z plane. As the angle increases, particles start to roll down along the inclined surface (Figure 6b). When the inclination angle is sufficiently large, particles at the top cascade down to the bottom of the drum (Figure 6c). As the drum rotation continues, this process repeats and the particles are mixing and making contact with each other. Various types of particles show similar kinematic behaviours. The fill ratio defined as the total volume of the particles divided by the volume of the drum is calculated and given in Table 1. Clearly, with a smaller particle volume, the fill ratio is smaller, which results in a lower fill height of the granular bed.

3.2. The charge distribution

Figure 7 presents the charge distribution for the particle I of $D_{32} = 3.72 \times 10^{-4}$ m in the rotating drum at $t = 0.33$ s. It can be seen that the charge distribute non-uniformly in the granular bed. At the early stage of the drum rotation, the particles at the inclined surface of the granular bed possess little charge (Figure 7a). On the contrary, the charges of particles close to the drum wall are much higher. This indicates that the charges are initially generated from the contact between the particles and the drum wall at the region close to the drum surface. The charge is

also higher at the region near the side wall of the drum. In addition, the charge on each primary sphere varies, implying that the charge distribution of each particle is not uniform.

Figure 8 presents the charge evolution for the particle I ($D_{32} = 3.72 \times 10^{-4}$ m) in the granular bed during the drum rotation from the A-A view as indicated in Figure 7. It clearly shows that the charge is initially generated at the layer close to the cylindrical surface of the drum (Figure 8a), which is corresponding to Figure 7. As the drum rotates, the charged particles move with the drum to the top of the granular bed (Figure 8b) and then roll down along the inclined surface of the granular bed, which cause the particles to mix with each other and charge transfer between particles. The charge in the granular bed gradually evolves from the region near the drum walls to the inclined surface of the granular bed. The charge distribution eventually becomes uniform and the charges of the particles are saturated as indicated in Figure 8c.

Figure 9 shows the charge distribution in the drum with various particles at $t = 1.6$ s from the A-A view as indicated in Figure 7. Comparing with Figure 8b, the charge distribution for various shaped particles appears to be similar in the drum. The charge of the particles close to the walls of the drum is higher and the charge of the particles close to the inclined surface of the granular bed is lower except the spherical particles (Figure 9d). However, the saturation levels of the charges for various shaped particles are different at the same time instant. Specifically, the particles with a larger SMD accumulates less charge compared with their own equilibrium value as shown in Figures 9a, 9b and 9c. This indicates that particle shape can affect the charging transfer rate.

The charge density distribution is further determined and mapped on the polar coordinate. The centres of all primary spheres are projected onto the z - y plane along x direction in polar coordinates as shown in Figure 10. As only the centres of the primary spheres are projected on the polar coordinate and a small number of particles is used, a few layers of the centres of the primary spheres are shown in Figure 10. To show the contour of charge density distribution continuously in the radial direction, a relatively large grid size and a small number of grids (5 layers) in radial direction was chosen. In this study, the polar coordinate with the radius of 0.0015 m is divided into 5×20 grids in the radial and circumferential directions respectively as in Figure 10. In each grid, the charge density can be defined as:

$$\sigma_g = \frac{\sum_{i=1}^{n_s} q_{si}}{A_g} \quad (8)$$

where A_g is the grid area; q_{si} is the charge of the primary sphere of which the centre is mapped into the corresponding grid; n_s is the number of primary spheres mapped into this grid. It can be seen that the charge density represents the charge concentration of this grid along the x axial direction.

Figure 11 presents the evolution of the charge density distribution ($\text{C} \cdot \text{m}^{-2}$) for the particle I ($D_{32} = 3.72 \times 10^{-4}$ m). It is clear that the charge is initially generated from the region close to the drum wall (Figure 11a) and then evolves to the inclined surface of the granular bed until the charge density of the particles reaches the equilibrium value (Figures 11b, 11c and 11d).

Figure 12 shows the charge density distribution of various particles in the drum at $t = 1.6$ s. Particles with different shapes present different charge density distributions. For the particles

with larger SMDs and larger sphericity, the charge density concentrates at the cylindrical surface of the drum and the saturation level of the charge is relatively smaller (Figures 12a and 12b). However, for the particles with a smaller SMD, a higher charge density in the entire granular bed is obtained (Figure 12c). Exceptionally, the charge density of the spherical particles is much higher than the other particles.

3.3. The charge accumulation

Figure 13 shows the charge accumulation processes for various particles during the drum rotation. The charge gradually increases and reaches an equilibrium state. However, the equilibrium charges of particles vary with different D_{32} . Specifically, for the particles with the same D_{max} , a larger D_{32} leads to a greater equilibrium charge. Figure 14 shows the corresponding evolution of the charge-to-mass ratio of the various particles. It can be seen that the equilibrium charge-to-mass ratio of the particles also varies with D_{32} . However, a larger D_{32} leads to a smaller equilibrium charge-to-mass ratio.

4. Discussions

4.1 Surface charge density for particles with same D_{max} and D_v

The charge distribution of various shaped particles in the rotating drum shows a similar pattern despite the different fill ratios and that the particles have the same material properties. Because of the contact potential difference between the particles and the drum, the charge is initially transferred between the particles and the drum wall as shown in Figure 8a rather than between particles. Moreover, the particles move with the drum as it rotates due to the friction

between the particles and the drum until the inclination angle of the granular bed is sufficiently large that the particles at the top start to roll down to the bottom. The charged particles are mixed in the granular bed and make contacts with other particles, which promotes charge transfer. As the charge on particles accumulates, all particles are eventually charged to an equilibrium state (Figure 13). Hence it can be seen that the charge of the granular bed gradually increases from the region near the wall of the drum to the inclined surface of the granular bed as shown in Figure 8 and Figure 11.

The charge of particles gradually increases to an equilibrium value. However, the equilibrium charge of particles depends on particle shape. According to Eq. (4), the equilibrium charge of a particle is proportional to the surface area of the particle, implying that the equilibrium mean surface charge densities of particles with different D_{32} are equal [20]. In addition, the mean surface charge density during the process can be defined as a function of time as follows:

$$\sigma_p = \sigma_{p0} e^{-k_c t} + \sigma_{p\infty} (1 - e^{-k_c t}) \quad (9)$$

where σ_{p0} and $\sigma_{p\infty}$ are the initial mean surface charge density and the equilibrium mean surface charge density and k_c is the charging coefficient.

Figure 15 shows the evolution of the mean surface charge density of various particles. The solid line is the fitting line of Eq. (9). The mean surface charge density of the particles increases exponentially to the same equilibrium state with different charging coefficients. The charging coefficients and the related SMDs and sphericity are listed in Table 4. Generally, for particles with the same D_{max} , a smaller D_{32} and sphericity leads to a larger charging

coefficient, which means that a particle with a smaller D_{32} will become charged more rapidly than those with a larger D_{32} . Although particles have the same maximum diameter, a smaller D_{32} leads to a smaller particle volume and a smaller fill ratio as shown in Table 1. Due to the smaller fill ratio, particles with a smaller D_{32} can mix more effectively in the rotating drum. In addition, a smaller D_{32} leads to a larger surface-to-volume ratio, and relatively more contacts on the surface of the particle. Therefore, for particles with the same D_{max} , a smaller D_{32} results in a faster charge accumulation.

However, particles with the same equivalent volume diameter but different shapes have different charge accumulation behaviour from those with the same maximum diameter. The model setup of the charge accumulations for the particles with the same equivalent volume diameter is the same as in Section 2.3 and Table 2.

Figure 16 shows the mean surface charge density of various particles with the same D_v . Once again, the solid line is the fitting line of Eq. (9). The mean surface charge density of various particles increases exponentially to the same equilibrium value. Generally, for particles with the same D_v , the surface charge density of particles with a larger D_{32} ($D_{32} = 3.16 \times 10^{-4}$ m) increase faster than that with a smaller D_{32} ($D_{32} = 3.03 \times 10^{-4}$ m), indicating that a larger D_{32} can lead to a faster charge accumulation. However, it is found that the surface charge density of particles with $D_{32} = 2.99 \times 10^{-4}$ m increases faster than that with $D_{32} = 3.03 \times 10^{-4}$ m. In addition, the differences between the charging coefficients of various particles with the same D_v (Table 5) are relatively small, compared with those for various particles with the same maximum diameter (Table 4).

The effect of D_{32} for various particles with the same D_v on the charging process is different from that with the same maximum diameter. In Section 2.3, a smaller D_{32} leads to a smaller particle volume and a smaller fill ratio. Due to the smaller fill ratio, particles with a smaller D_{32} can mix more effectively in the rotating drum and get charged more rapidly. In this section for particles with the same D_v , the fill ratios in the rotating drum for various particles are identical. Therefore, the differences between the charging coefficients of various particles with the same D_v are relatively small. In addition, a larger D_{32} lead to a larger sphericity. Particles with larger sphericity may tend to rotate and roll in the rotating drum more easily, which can result in a faster charging process. However, it can be seen that the difference between the charging coefficients is relatively small in this case.

The charge distribution and accumulation of particles in this numerical study are in broad agreements with experimental investigations reported in the literature. During the drum rotation, the charge propagates from the wall to the centre. This is consistent with the experimental observation [12] that the charge is larger on the particles close to the wall surface when they flow through a metal cylinder. The charge and charge-to-mass ratio can reach equilibrium after a period of mixing or blend as shown experimentally [39,40]. In addition, the smaller particles tend to have a faster charging process and a higher charge level (net charge or charge-to-mass ratio), as predicted by this current study. However, Šupuk et al. [41] suggested that when the electrostatic interactions between particles and space charge effects on the charge transfer are considered, the level of equilibrium charge can be reduced. Therefore, the electrostatic interactions [42] and space charge effects need to be considered in future studies, especially for fine particles and binary mixtures.

4.2 The intra-particle charge distribution

In this study, the particle shape is represented by 8 primary spheres. During the process, the charge on each primary sphere of the (multi-sphere) particle varies, especially at the earlier stage (Figure 17). In other words, the non-uniform intra-particle charge distribution is observed. To characterise the intra-particle charge distribution, the mean relative intra-particle charge deviation is defined as:

$$\tau = \frac{\sqrt{\frac{1}{n_{sp}} \sum_{i=1}^{n_{sp}} (\bar{q}_{si} - \bar{q}_s)^2}}{\bar{q}_s}$$

where n_{sp} is the number of primary spheres in each (multi-sphere) particle, which is 8 in the current study; \bar{q}_{si} is the mean charge of all primary spheres with the index of i within each multi-sphere ($n_{sp} = 8$); \bar{q}_s is the mean charge of all primary spheres in the particle system. The mean relative intra-particle charge deviation represents the ratio of mean charge deviation within multi-spheres to the mean charge of all primary spheres. A smaller value means that the charge distributes more uniformly on the multi-sphere particles while a larger value indicates that the charge on the primary spheres with specific indices is largely different from other primary spheres in the particle system.

Figure 18 shows the evolution of the relative intra-particle charge deviation of particles with the same maximum diameter and equivalent volume diameter. Initially, the charge of particles is zero and the deviation is also zero. When the drum starts to rotate, the deviation increases rapidly. This is because that only a few primary spheres on particles collide with the cylindrical surface of the drum and get charged earlier than others as shown in Figure 8a.

These primary spheres are non-uniformly distributed and consequently a larger relative intra-particle charge deviation occurs. However, when particles start to move with the rotation of the drum, they mix and collide with each other. The deviation decreases rapidly to a negligible level. For instance, the value of the deviation is smaller than 5% within less than 1 s. Generally, in the particle system, the charge distributes uniformly over primary spheres for all multi-sphere particles. However, it should be noted that non-uniform charge distribution on each individual multi-sphere is still observed. This implies that all primary spheres in the particle system have similar probability to acquire charge, but the primary spheres within each multi-sphere can be charged differently (Figure 17). Both particles with the same maximum diameter and equivalent volume diameter show similar evolution pattern on the relative intra-particle charge deviation.

An exceptional case in this study is that the spherical particles ($D_{32} = 4.00 \times 10^{-4}$ m) have a larger charging coefficient, compared with the particles of $D_{32} = 3.72 \times 10^{-4}$ m, although both particles have a similar shape (D_{32} and sphericity). The spherical particle ($D_{32} = 4.00 \times 10^{-4}$ m) is treated as one sphere with a uniform charge distribution on the surface and the induced potential difference is determined by the uniform distribution [13]. However, the multi-sphere particle is treated as an assembly of primary spheres on which the non-uniform charge distribution is observed, as shown in Figure 18. Matsuyama *et al.* [22] suggested that the induced potential difference is mainly affected by the local initial charge at the contact area while the charge at the remote (rear) side to the contact area has less effect on the induced potential difference. Therefore, for particles approximated using multi-spheres, the induced potential difference is only determined by the charge on the local primary sphere (Eq. (2)). Consequently, the charging coefficients of the spherical particle ($D_{32} = 4.00 \times 10^{-4}$ m) and the multi-sphere particle ($D_{32} = 3.72 \times 10^{-4}$ m) are different. This implies that the charging process

of particles with non-uniform intra-particle charge distribution is different from the particles with uniform intra-particle charge distribution. In this study, the particle shape is represented using only 8 primary spheres. A more accurate approximation and the effect of the number of primary spheres, e.g. more primary spheres for one particle, needs to be considered. In addition, how particle shape alter the mode of contact (sliding, bouncing and rotating) [21, 43, 44] and the relevant charging process also need further investigation.

5. Conclusions

In this study, a sphere-tree multi-sphere method and a contact electrification model are implemented into the DEM to simulate the charging process of irregular particles in a rotating drum. The charge distribution and accumulation of irregular particles are investigated. For all particles, the charge transfer originated from the contact between a particle and the drum because of the contact potential difference. The charge is initially concentrated at the region near the drum wall and then propagates to the entire granular bed. Particles with the same maximum diameter, smaller SMD and sphericity have a larger charging coefficient, which leads to a faster charge accumulation. Eventually, all particles with various SMDs obtain the same surface charge density. However, for particles with the same equivalent volume diameter, it is found that the charging coefficients are relatively similar due to the same fill ratio. The non-uniform intra-particle charge distribution is observed for each individual multi-sphere particle during the charge accumulation process. It is clear that the particle shape plays an important role in charge transfer during powder handling processes.

References

- [1] A.G. Bailey, Electrostatic phenomena during powder handling, *Powder Technol.* 37 (1984) 71–85.
- [2] S. Matsusaka, H. Maruyama, T. Matsuyama, M. Ghadiri, Triboelectric charging of powders: A review, *Chem. Eng. Sci.* 65 (2010) 5781–5807.
- [3] M.I. Kornfeld, Frictional electrification, *J. Phys. D. Appl. Phys.* 9 (1976) 1183–1192.
- [4] C. Liu, A.J. Bard, Electrons on dielectrics and contact electrification, *Chem. Phys. Lett.* 480 (2009) 145–156.
- [5] J.Q. Feng, D.A. Hays, Relative importance of electrostatic forces on powder particles, *Powder Technol.* 135 (2003) 65–75.
- [6] Y. Pu, M. Mazumder, C. Cooney, Effects of electrostatic charging on pharmaceutical powder blending homogeneity, *J. Pharm. Sci.* 98 (2009) 2412–2421.
- [7] B.A. Grzybowski, A. Winkleman, J.A. Wiles, Y. Brumer, G.M. Whitesides, Electrostatic self-assembly of macroscopic crystals using contact electrification., *Nat. Mater.* 2 (2003) 241–245. doi:10.1038/nmat860.
- [8] C. Pei, C.-Y. Wu, S. Byard, D. England, Numerical analysis of electrostatic effects during powder deposition using DEM/CFD, *J. Pharm. Pharmacol.* 62 (2010) 1454–1455.
- [9] E.N. Nwose, C. Pei, C.-Y. Wu, Modelling die filling with charged particles using DEM/CFD, *Particuology.* 10 (2012) 229–235.
- [10] S.C. Wu, D.T. Wasan, A.D. Nikolov, Two-Dimensional Self-Assembly of Similarly Charged Granular Particles, *Ind. Eng. Chem. Res.* 47 (2008) 5005–5015.
- [11] M. Nifuku, H. Katoh, A study on the static electrification of powders during pneumatic transportation and the ignition of dust cloud, *Powder Technol.* 135-136 (2003) 234–242. doi:10.1016/S0032-5910(03)00163-3.

- [12] K.R. LaMarche, X. Liu, S.K. Shah, T. Shinbrot, B.J. Glasser, Electrostatic charging during the flow of grains from a cylinder, *Powder Technol.* 195 (2009) 158–165.
- [13] C. Pei, C.-Y. Wu, D. England, S. Byard, H. Berchtold, M. Adams, Numerical analysis of contact electrification using DEM–CFD, *Powder Technol.* 248 (2013) 34–43. doi:10.1016/j.powtec.2013.04.014.
- [14] J. Guardiola, V. Rojo, G. Ramos, Influence of particle size, fluidization velocity and relative humidity on fluidized bed electrostatics, *J. Electrostat.* 37 (1996) 1–20.
- [15] H.P. Zhu, Z.Y. Zhou, R.Y. Yang, A.B. Yu, Discrete particle simulation of particulate systems: Theoretical developments, *Chem. Eng. Sci.* 62 (2007) 3378–3396.
- [16] Y. Guo, K.D. Kafui, C.Y. Wu, C. Thornton, J.P.K. Seville, A coupled DEM/CFD analysis of the effect of air on powder flow during die filling, *AIChE J.* 55 (2009) 49–62.
- [17] K.D. Kafui, C. Thornton, M.J. Adams, Discrete particle-continuum fluid modelling of gas-solid fluidised beds, *Chem. Eng. Sci.* 57 (2002) 2395–2410.
- [18] J. Yao, C.-H. Wang, Granular size and shape effect on electrostatics in pneumatic conveying systems, *Chem. Eng. Sci.* 61 (2006) 3858–3874. doi:10.1016/j.ces.2006.01.015.
- [19] J. Yao, J. Wu, Y. Zhao, E.W.C. Lim, P. Cao, F. Zhou, et al., Experimental investigations of granular shape effects on the generation of electrostatic charge, *Particuology.* (2013) 1–8. doi:10.1016/j.partic.2013.01.010.
- [20] C. Pei, C.-Y. Wu, M. Adams, D. England, S. Byard, H. Berchtold, Contact electrification and charge distribution on elongated particles in a vibrating container, *Chem. Eng. Sci.* 125 (2014) 238–247. doi:10.1016/j.ces.2014.03.014.
- [21] P.M. Ireland, Dynamic particle-surface tribocharging: The role of shape and contact mode, *J. Electrostat.* 70 (2012) 524–531. doi:10.1016/j.elstat.2012.08.004.

- [22] T. Matsuyama, M. Ogu, H. Yamamoto, J.C.M. Marijnissen, B. Scarlett, Impact charging experiments with single particles of hundred micrometre size, *Powder Technol.* 135-136 (2003) 14–22.
- [23] J.F. Favier, M.H. Abbaspour-Fard, M. Kremmer, A.O. Raji, Shape representation of axisymmetrical, non-spherical particles in discrete element simulation using multi-element model particles, *Eng. Comput.* 16 (1999) 467–480.
- [24] G. Bradshaw, C. O’Sullivan, Sphere-tree construction using dynamic medial axis approximation, in: *Proc. 2002 ACM SIGGRAPH/Eurographics Symp. Comput. Animat.*, ACM, New York, USA, 2002: pp. 33–40. doi:10.1145/545261.545267.
- [25] G. Bradshaw, C. O’Sullivan, Adaptive medial-axis approximation for sphere-tree construction, *ACM Trans. Graph.* 23 (2004) 1–26. doi:10.1145/966131.966132.
- [26] R. Wang, K. Zhou, J. Snyder, X. Liu, H. Bao, Q. Peng, et al., Variational sphere set approximation for solid objects, *Vis. Comput.* 22 (2006) 612–621. doi:10.1007/s00371-006-0052-0.
- [27] B. Mirtich, Fast and Accurate Computation of Polyhedral Mass Properties, *J. Graph. Tools.* 1 (1996) 31–50. doi:10.1080/10867651.1996.10487458.
- [28] K.L. Johnson, *Contact Mechanics*, Cambridge University Press, Cambridge, 1985.
- [29] R.D. Mindlin, H. Deresiewicz, Elastic spheres in contact under varying oblique forces, *J. Appl. Mech. ASME.* 20 (1953) 327–344.
- [30] J. Lowell, A.C. Roseinnes, Contact electrification, *Adv. Phys.* 29 (1980) 947–1023.
- [31] T. Matsuyama, H. Yamamoto, Characterizing the electrostatic charging of polymer particles by impact charging experiments, *Adv. Powder Technol.* 6 (1995) 211–220.
- [32] S. Matsusaka, M. Ghadiri, H. Masuda, Electrification of an elastic sphere by repeated impacts on a metal plate, *J. Phys. D. Appl. Phys.* 33 (2000) 2311–2319.

- [33] T. Matsuyama, H. Yamamoto, Impact charging of particulate materials, *Chem. Eng. Sci.* 61 (2006) 2230–2238.
- [34] H. Watanabe, M. Ghadiri, T. Matsuyama, Y.L. Ding, K.G. Pitt, H. Maruyama, et al., Triboelectrification of pharmaceutical powders by particle impact, *Int. J. Pharm.* 334 (2007) 149–155.
- [35] M. Kremmer, J.F. Favier, A method for representing boundaries in discrete element modelling—part II: Kinematics, *Int. J. Numer. Methods Eng.* 51 (2001) 1423–1436. doi:10.1002/nme.185.
- [36] L. Li, W. Ma, Experimental study on the effective particle diameter of a packed bed with non-spherical particles, *Transp. Porous Media.* 89 (2011) 35–48. doi:10.1007/s11242-011-9757-2.
- [37] H. Wadell, Volume, shape and roundness of quartz Particles, *J. Geol.* 43 (1935) 250–280.
- [38] J.P.K. Seville, U. Tüzün, R. Clift, *Processing of particulate solids*, Blackie Academic & Professional, London, 1997.
- [39] D.A. Engers, M.N. Fricke, R.P. Storey, A.W. Newman, K.R. Morris, Triboelectrification of pharmaceutically relevant powders during low-shear tumble blending, *J. Electrostat.* 64 (2006) 826–835.
- [40] S. Karner, N.A. Urbanetz, Arising of electrostatic charge in the mixing process and its influencing factors, *Powder Technol.* 226 (2012) 261–268.
- [41] E. Šupuk, A. Hassanpour, H. Ahmadian, M. Ghadiri, Tribo-Electrification and Associated Segregation of Pharmaceutical Bulk Powders, *KONA Powder Part. J.* 29 (2011) 208–223.

- [42] C. Pei, C.-Y. Wu, D. England, S. Byard, H. Berchtold, M. Adams, DEM-CFD modeling of particle systems with long-range electrostatic interactions, *AIChE J.* (2015). doi:10.1002/aic.14768.
- [43] P.M. Ireland, Triboelectrification of particulate flows on surfaces: Part I -- Experiments, *Powder Technol.* 198 (2010) 189–198.
- [44] P.M. Ireland, Triboelectrification of particulate flows on surfaces: Part II -- Mechanisms and models, *Powder Technol.* 198 (2010) 199–210.

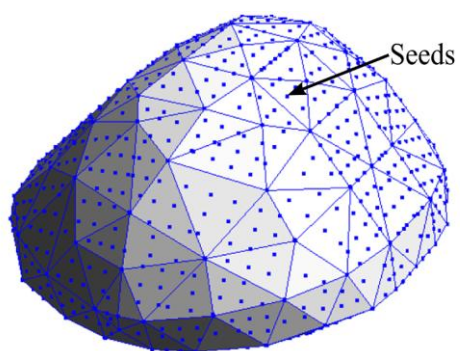


Fig. 1

ACCEPTED MANUSCRIPT

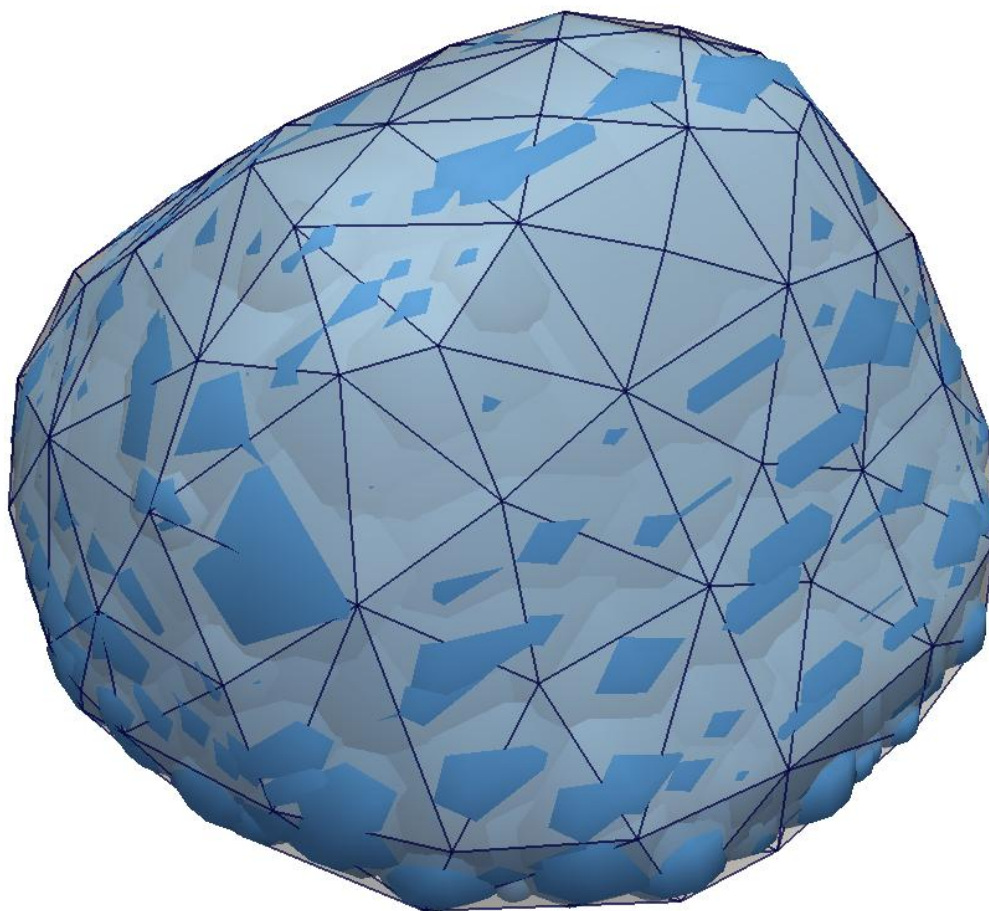


Fig. 2

ACCEP

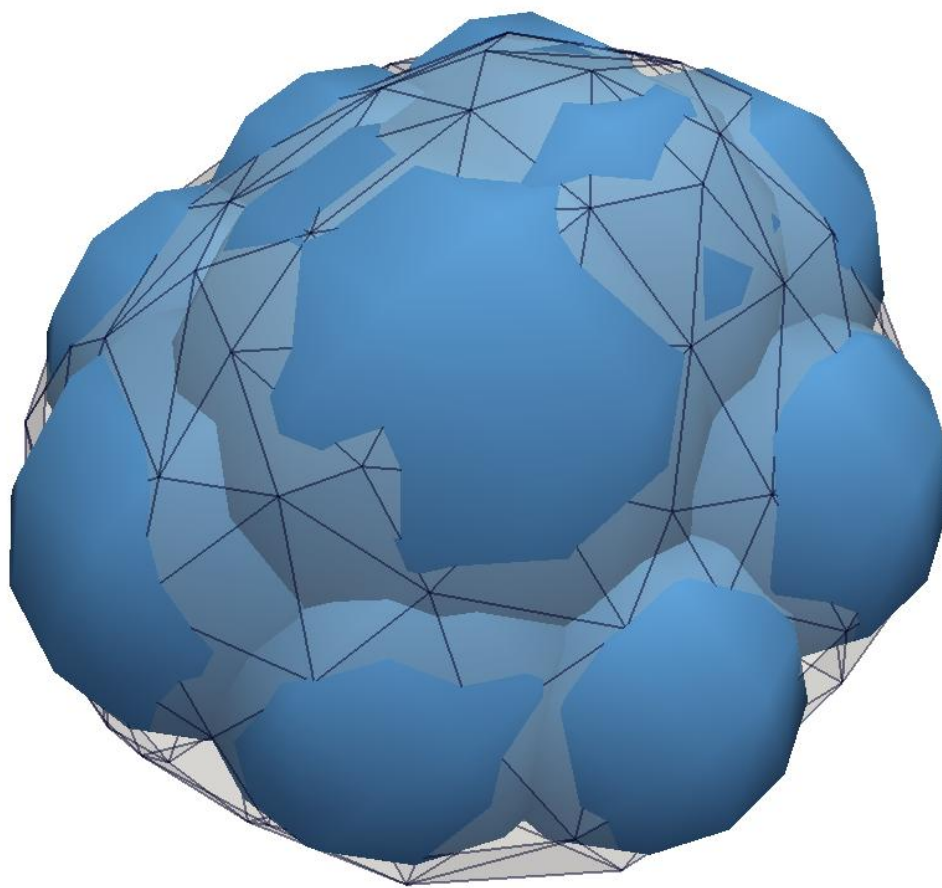


Fig. 3

ACCEP

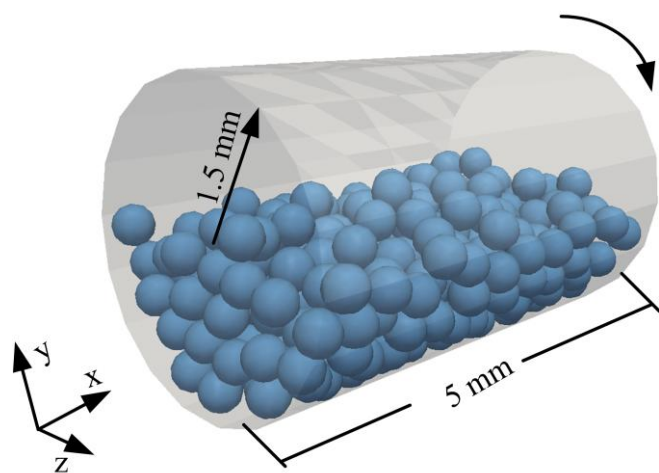
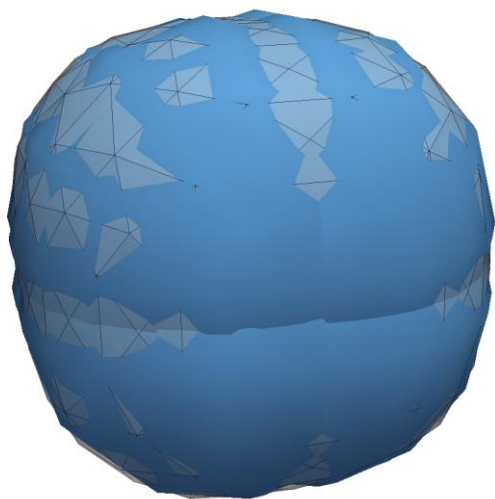


Fig. 4

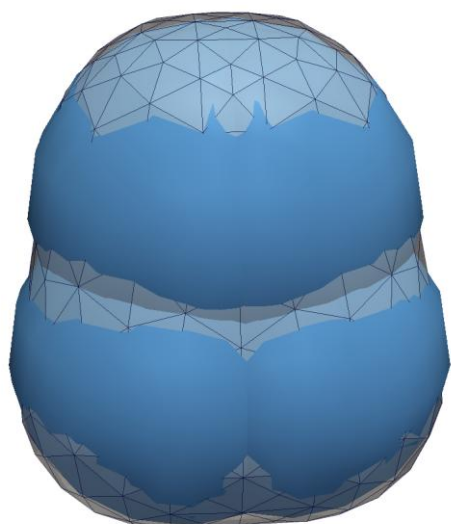
ACCEPTED MANUSCRIPT



(a) Particle I

Fig. 5a

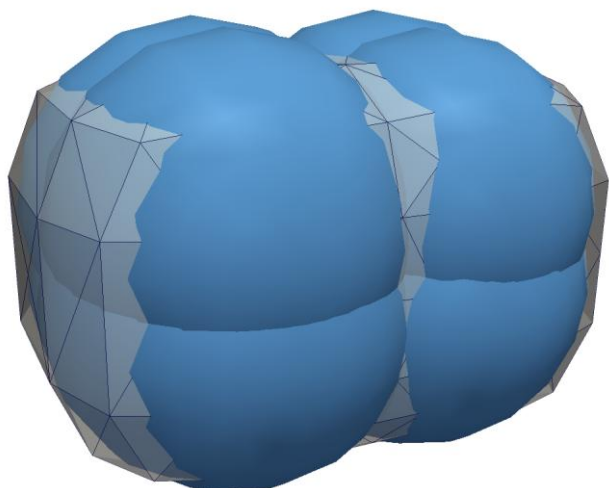
ACCEPTED MANUSCRIPT



(b) Particle II

Fig. 5b

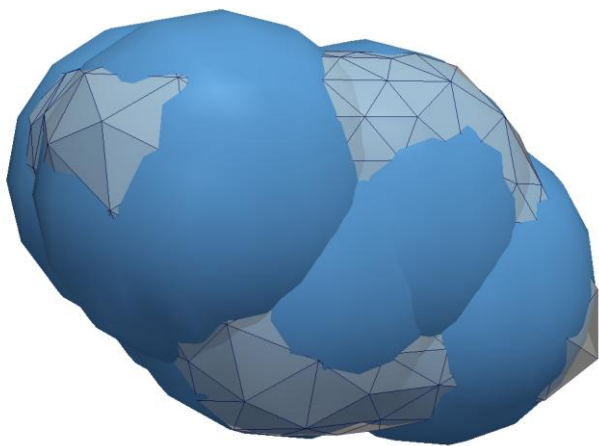
ACCEPTED MANUSCRIPT



(c) Particle III

Fig. 5c

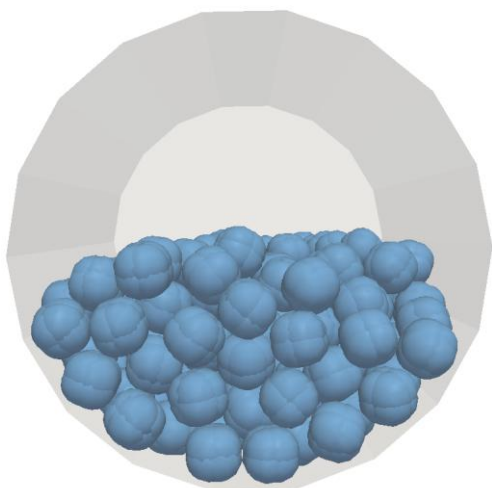
ACCEPTED MANUSCRIPT



(d) Particle IV

Fig. 5d

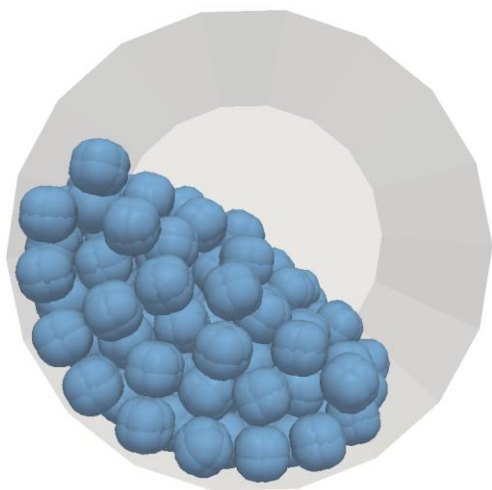
ACCEPTED MANUSCRIPT



(a) $t = 0.0$ s

Fig. 6a

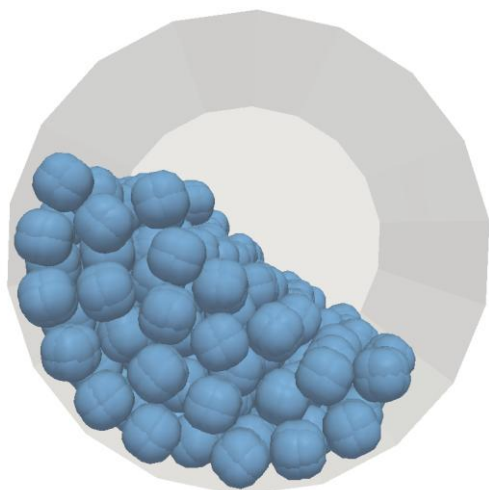
ACCEPTED MANUSCRIPT



(b) $t = 0.33$ s

Fig. 6b

ACCEPTED MANUSCRIPT



(c) $t = 0.63$ s

Fig. 6c

ACCEPTED MANUSCRIPT

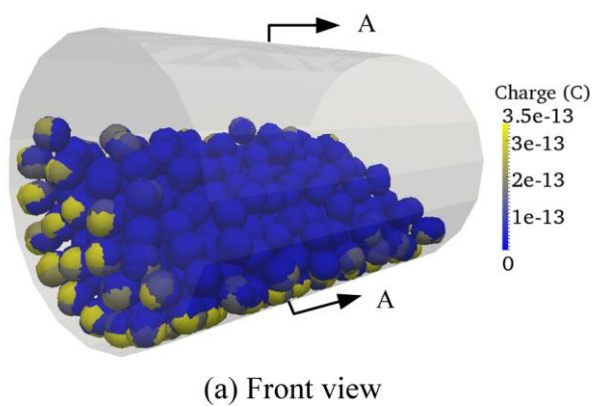
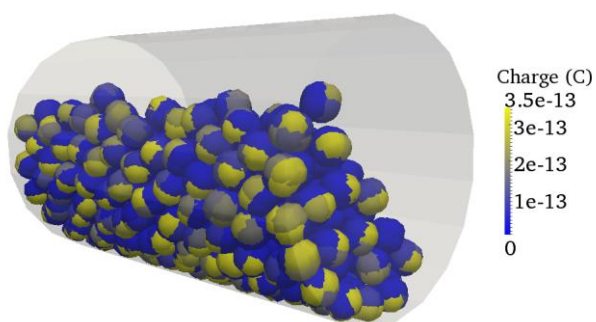


Fig. 7a

ACCEPTED MANUSCRIPT



(b) Back view

Fig. 7b

ACCEPTED MANUSCRIPT

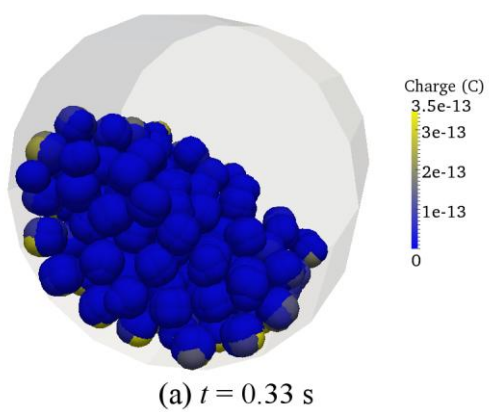
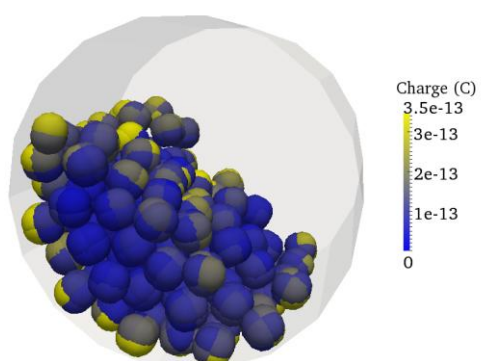


Fig. 8a

ACCEPTED MANUSCRIPT



(b) $t = 1.6$ s

Fig. 8b

ACCEPTED MANUSCRIPT

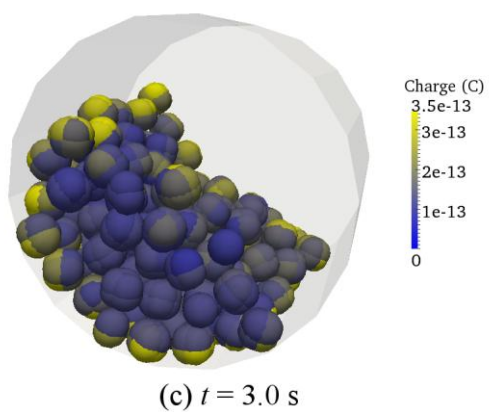


Fig. 8c

ACCEPTED MANUSCRIPT

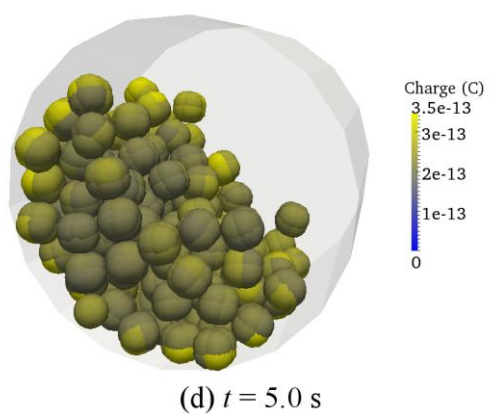
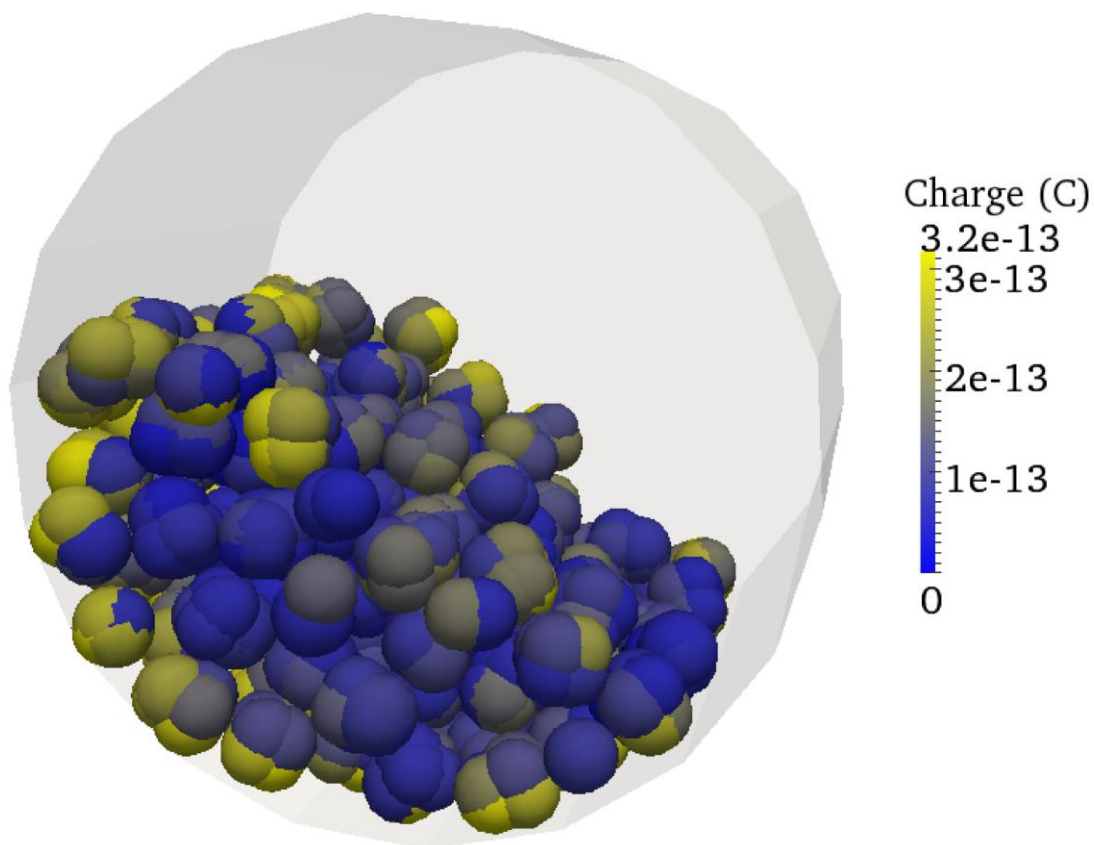


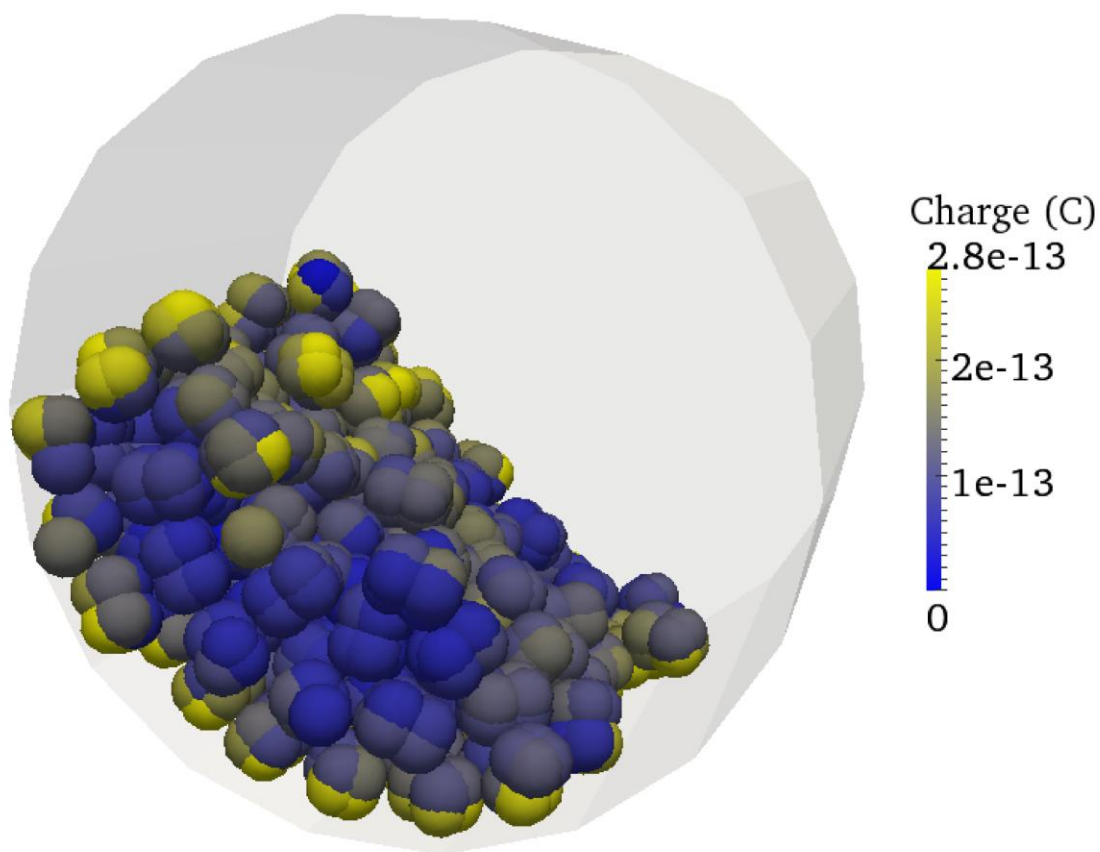
Fig. 8d

ACCEPTED MANUSCRIPT



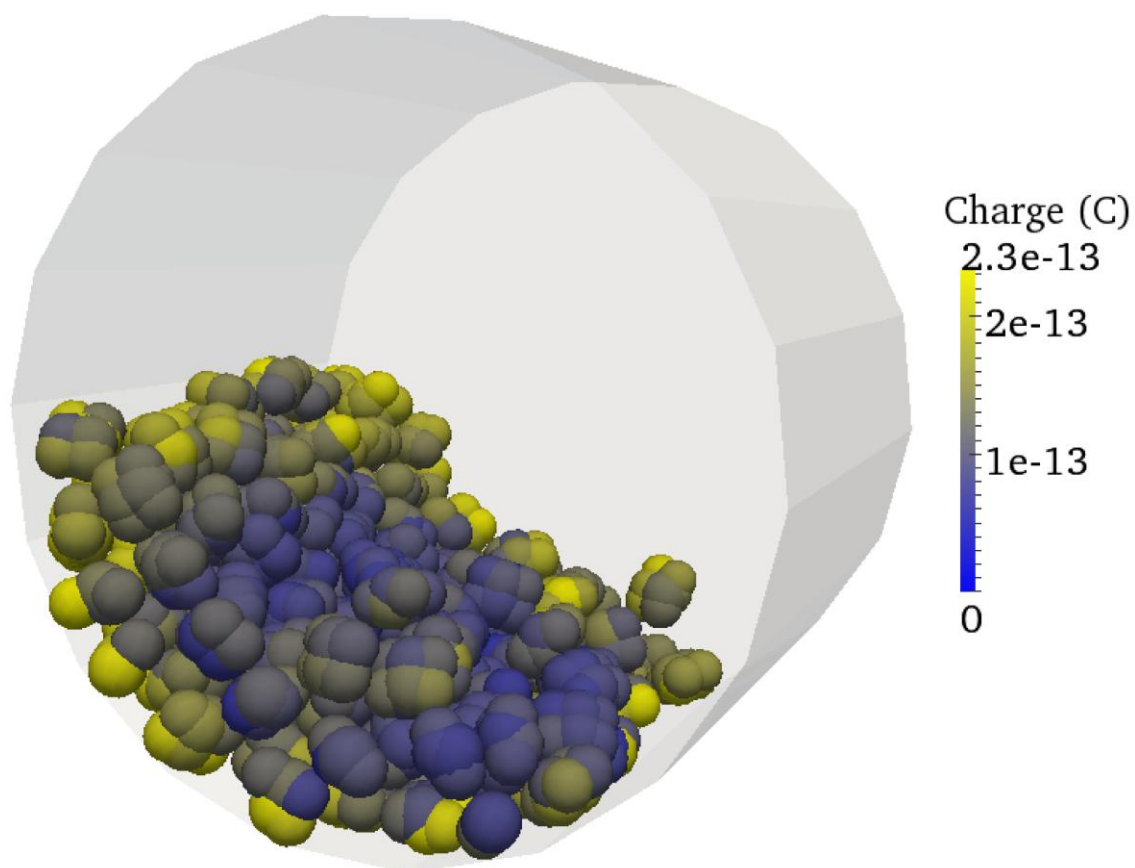
(a) Particle II ($D_{32} = 3.45 \times 10^{-4}$ m)

Fig. 9a



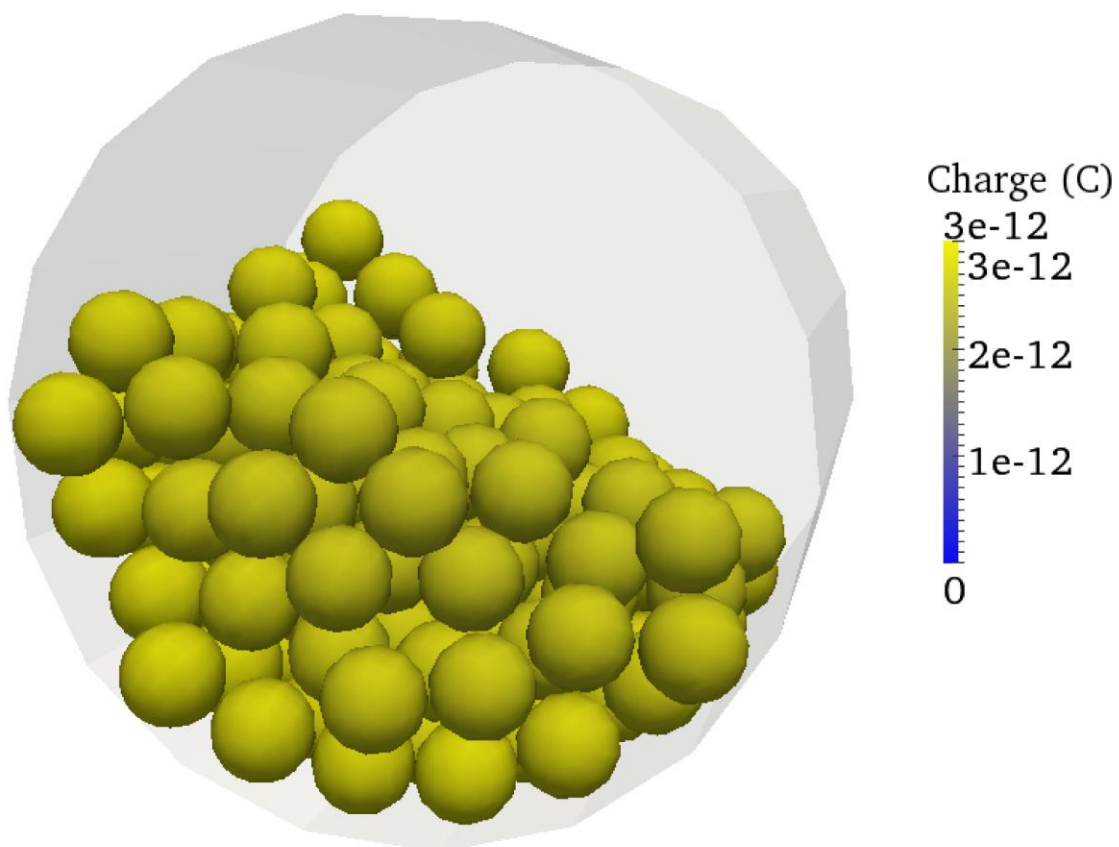
(b) Particle III ($D_{32} = 3.04 \times 10^{-4}$ m)

Fig. 9b



(c) Particle IV ($D_{32} = 2.71 \times 10^{-4}$ m)

Fig. 9c



(d) Sphere ($D_{32} = 4.0 \times 10^{-4}$ m)

Fig. 9d

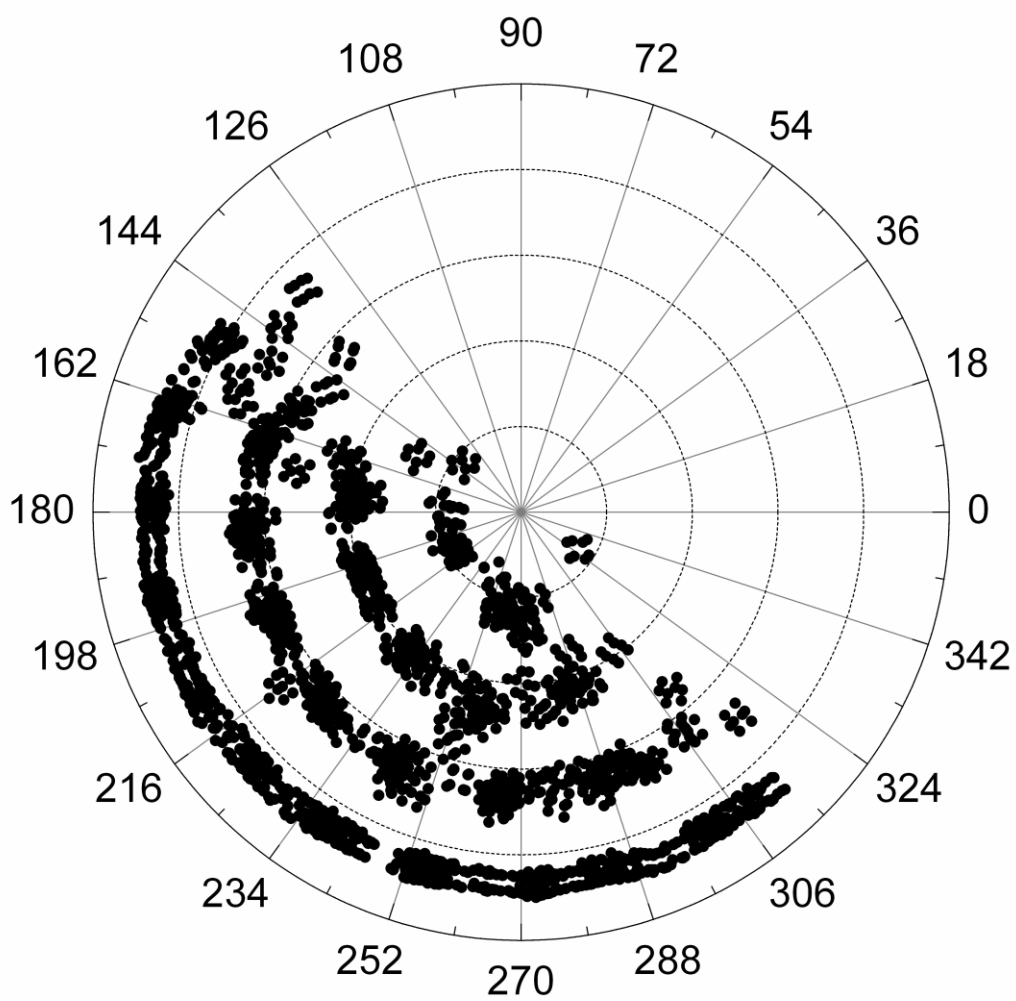
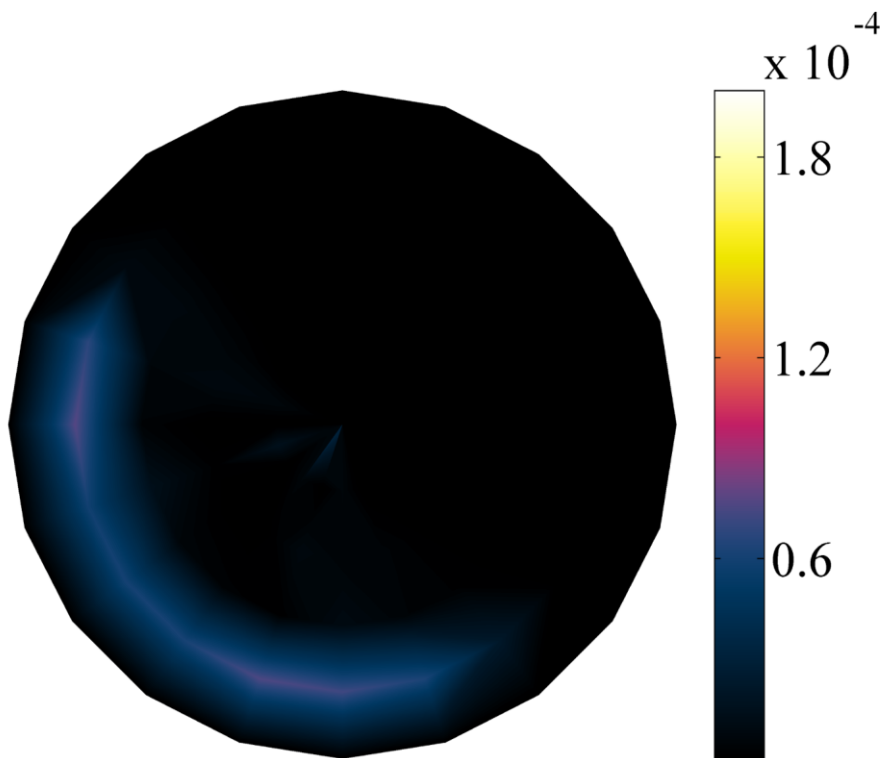


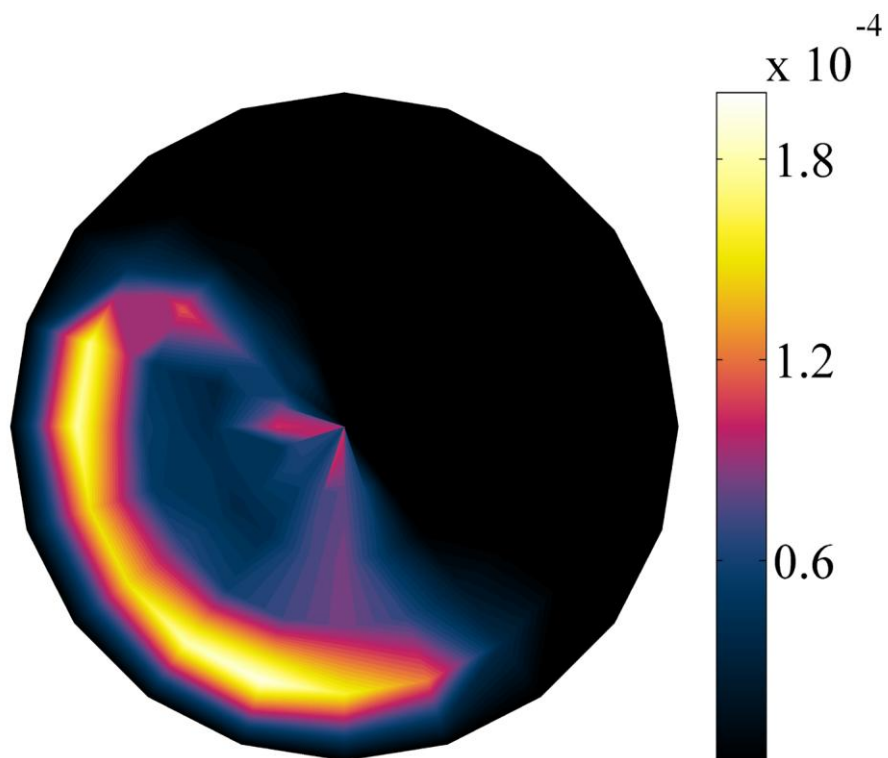
Fig. 10

AC



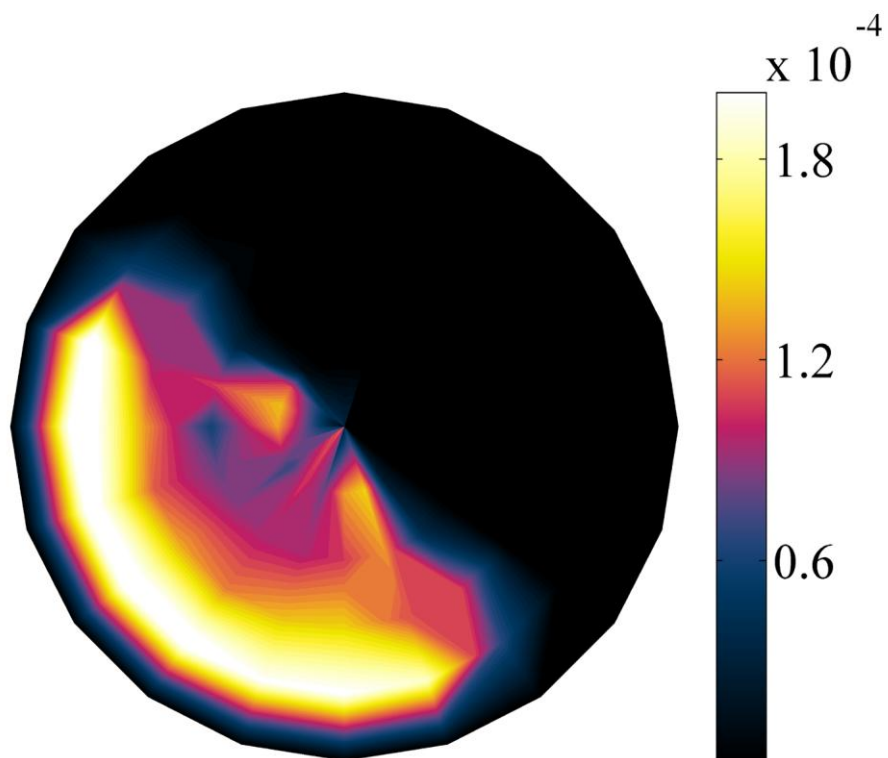
(a) $t = 0.33$ s

Fig. 11a



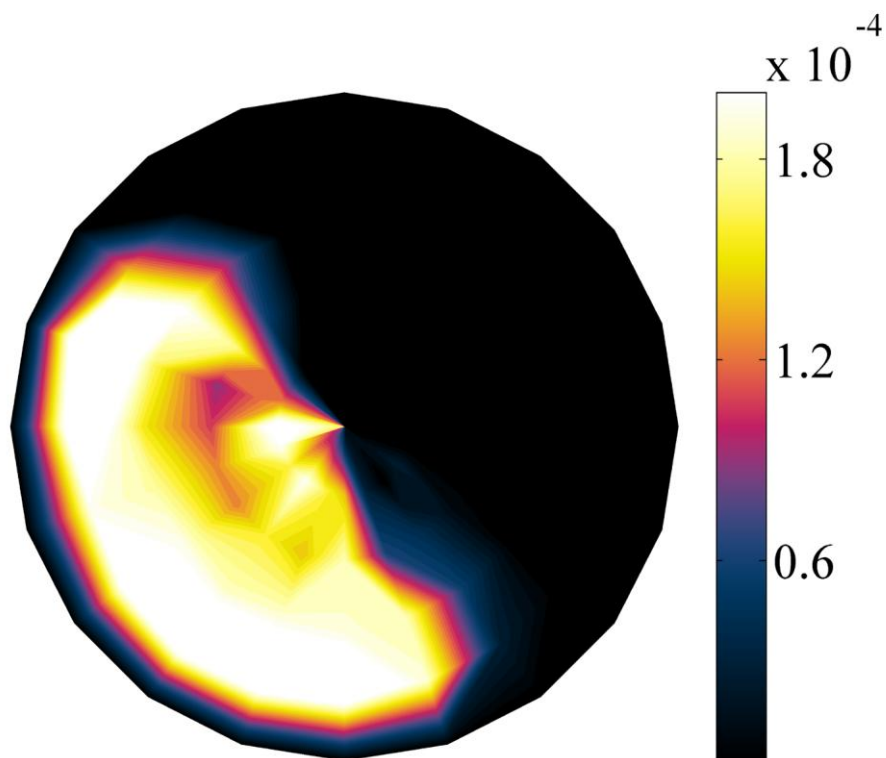
(b) $t = 1.6$ s

Fig. 11b



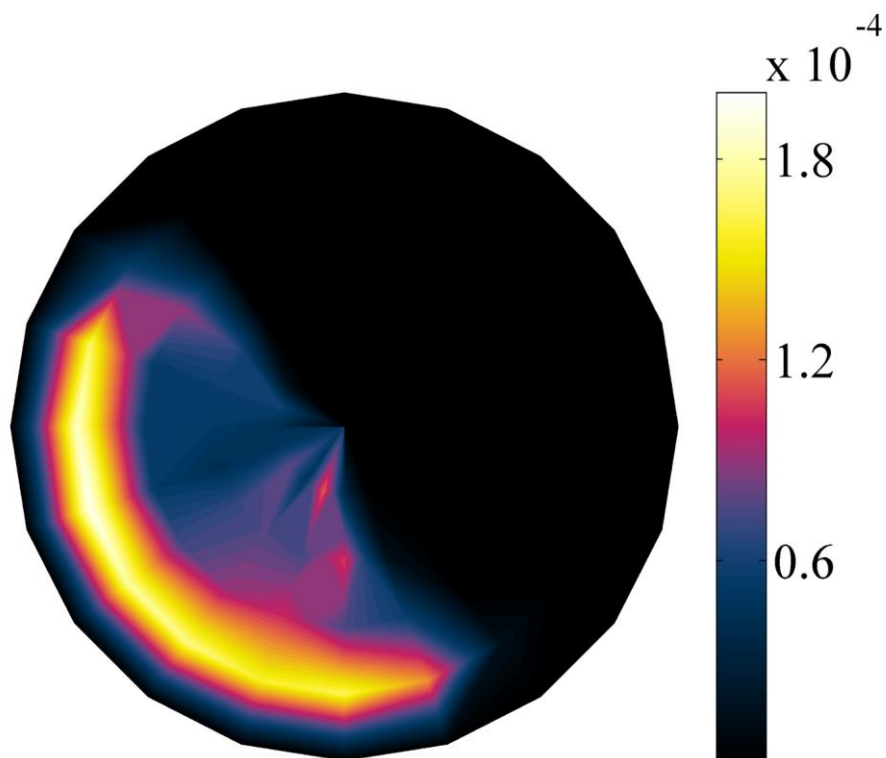
(c) $t = 3.0\text{s}$

Fig. 11c



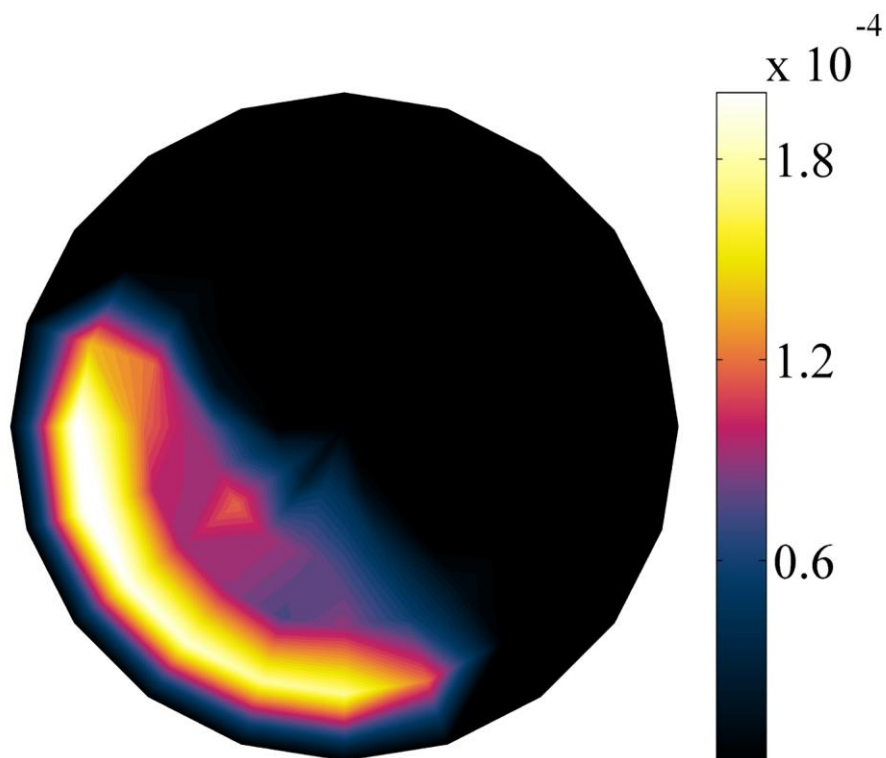
(d) $t = 5.0\text{s}$

Fig. 11d



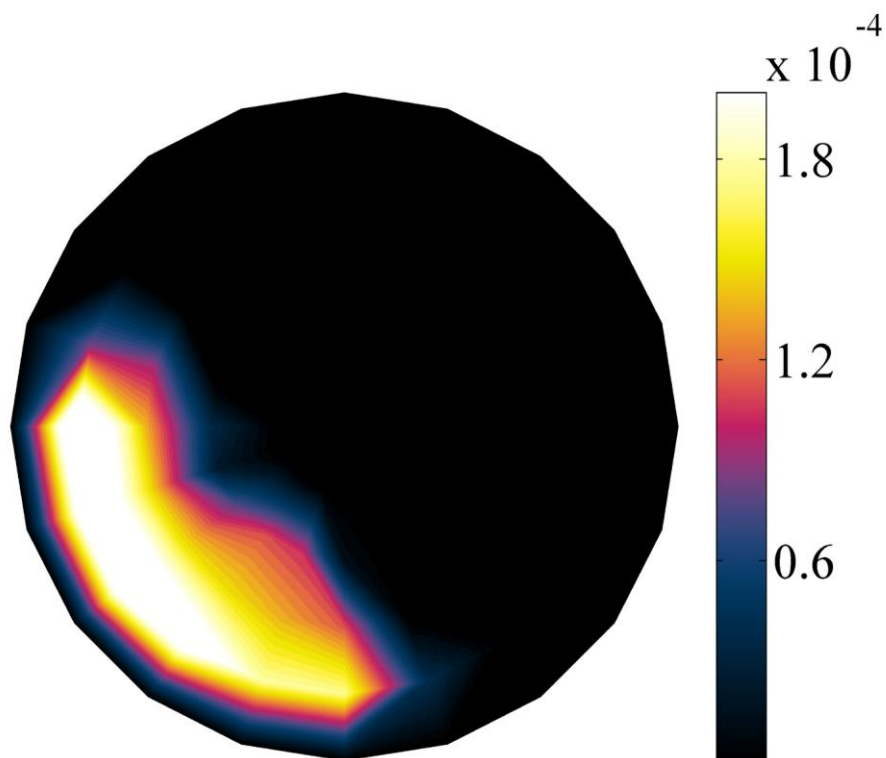
(a) Particle II ($D_{32} = 3.45 \times 10^{-4}$ m)

Fig. 12a



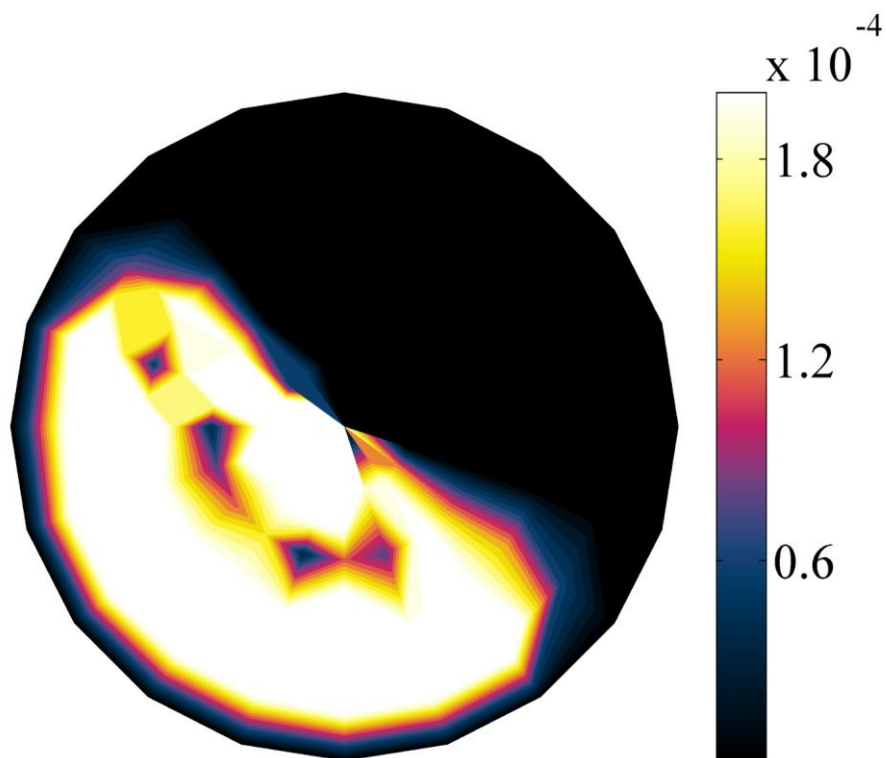
(b) Particle III ($D_{32} = 3.04 \times 10^{-4}$ m)

Fig. 12b



(c) Particle IV ($D_{32} = 2.71 \times 10^{-4}$ m)

Fig. 12c



(d) Sphere ($D_{32} = 4.0 \times 10^{-4}$ m)

Fig. 12d

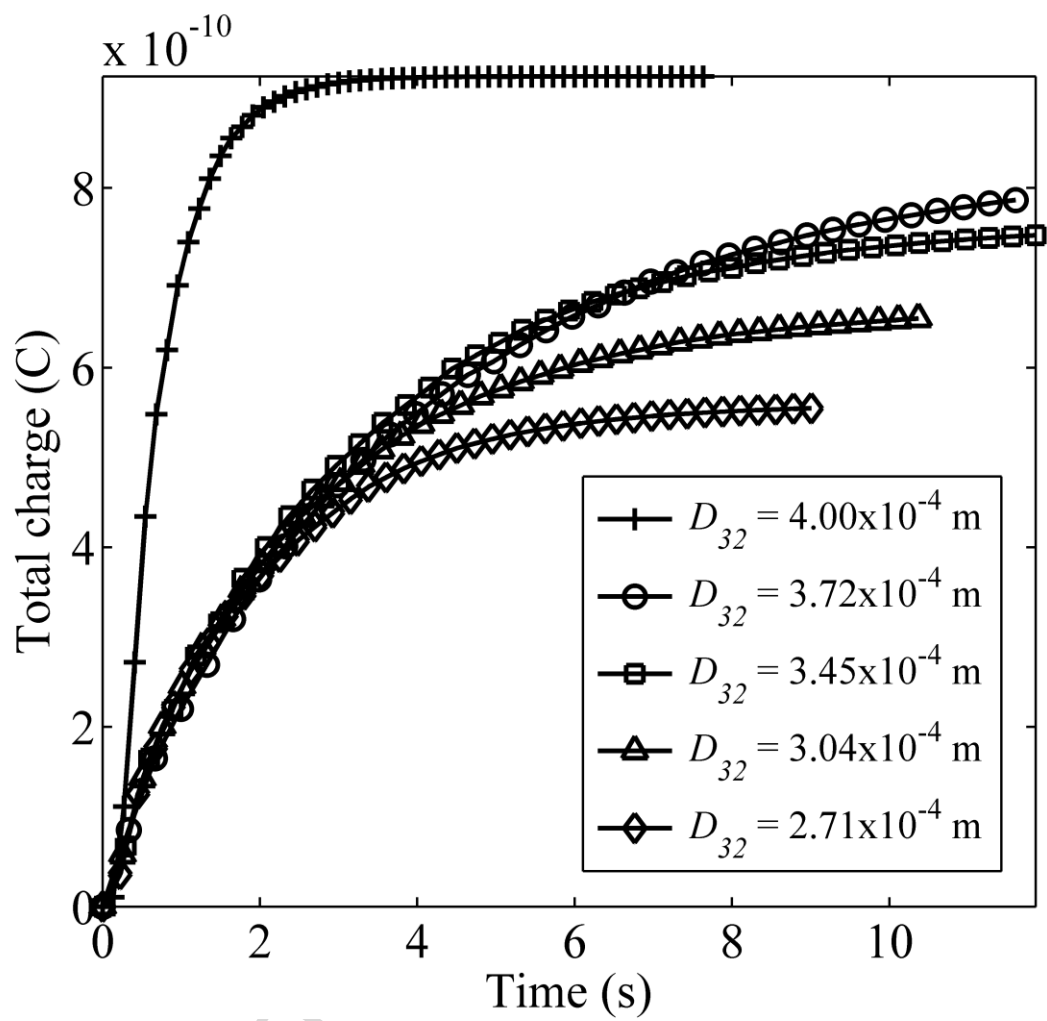


Fig. 13

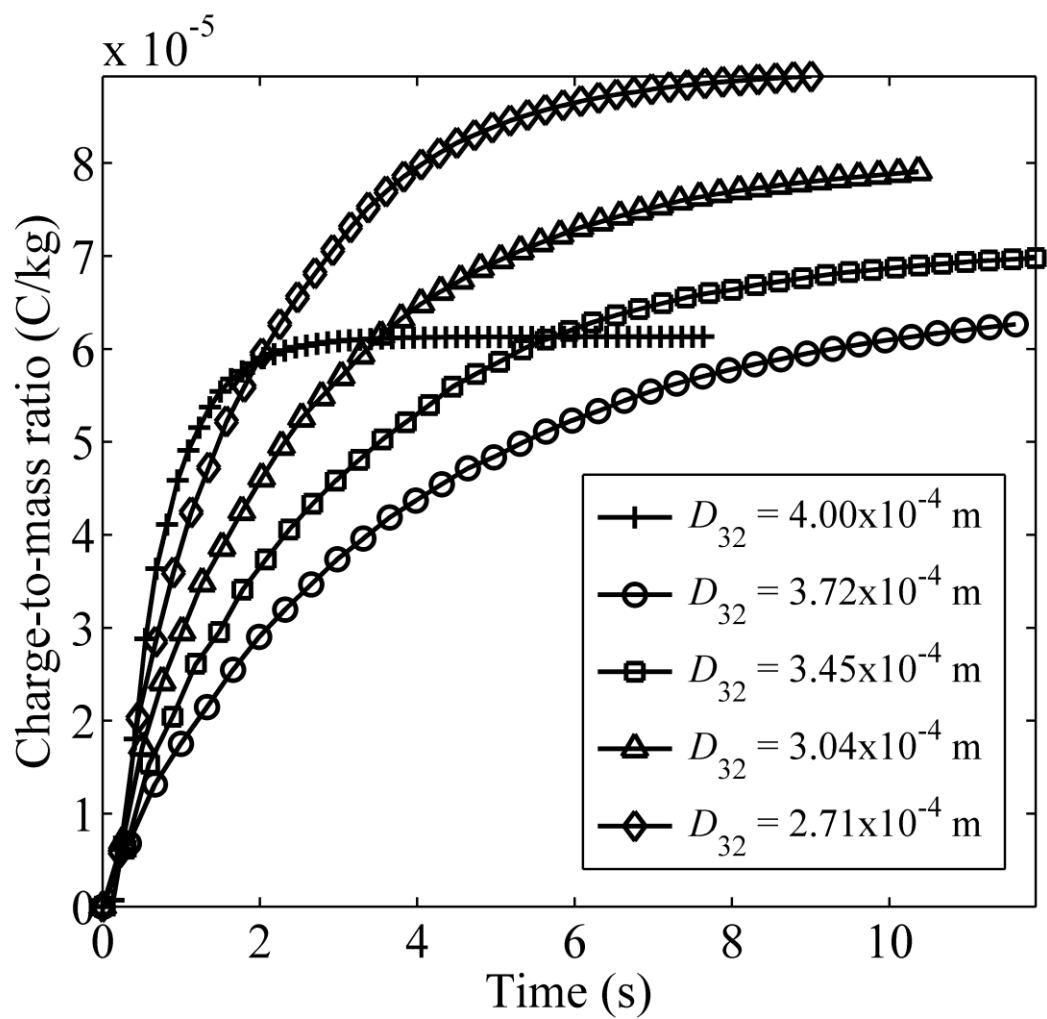


Fig. 14

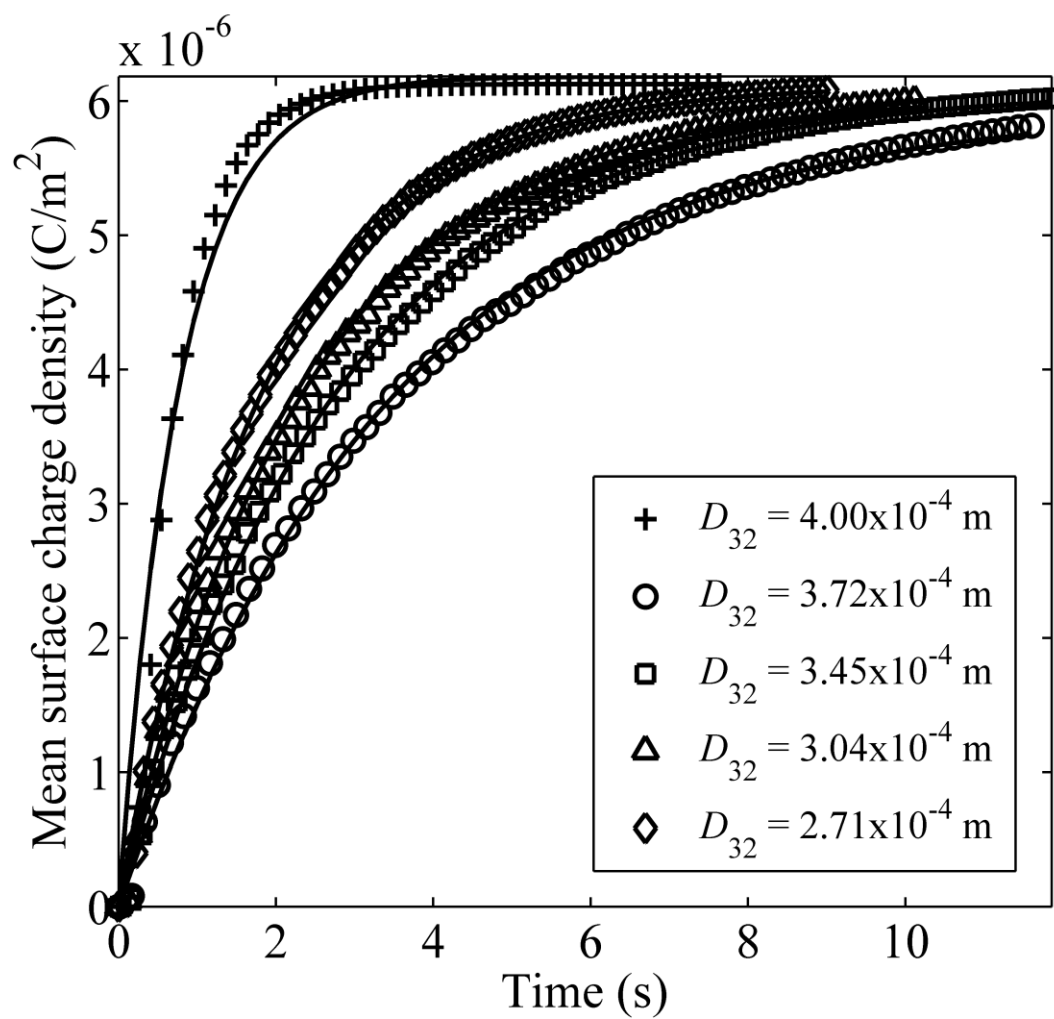


Fig. 15

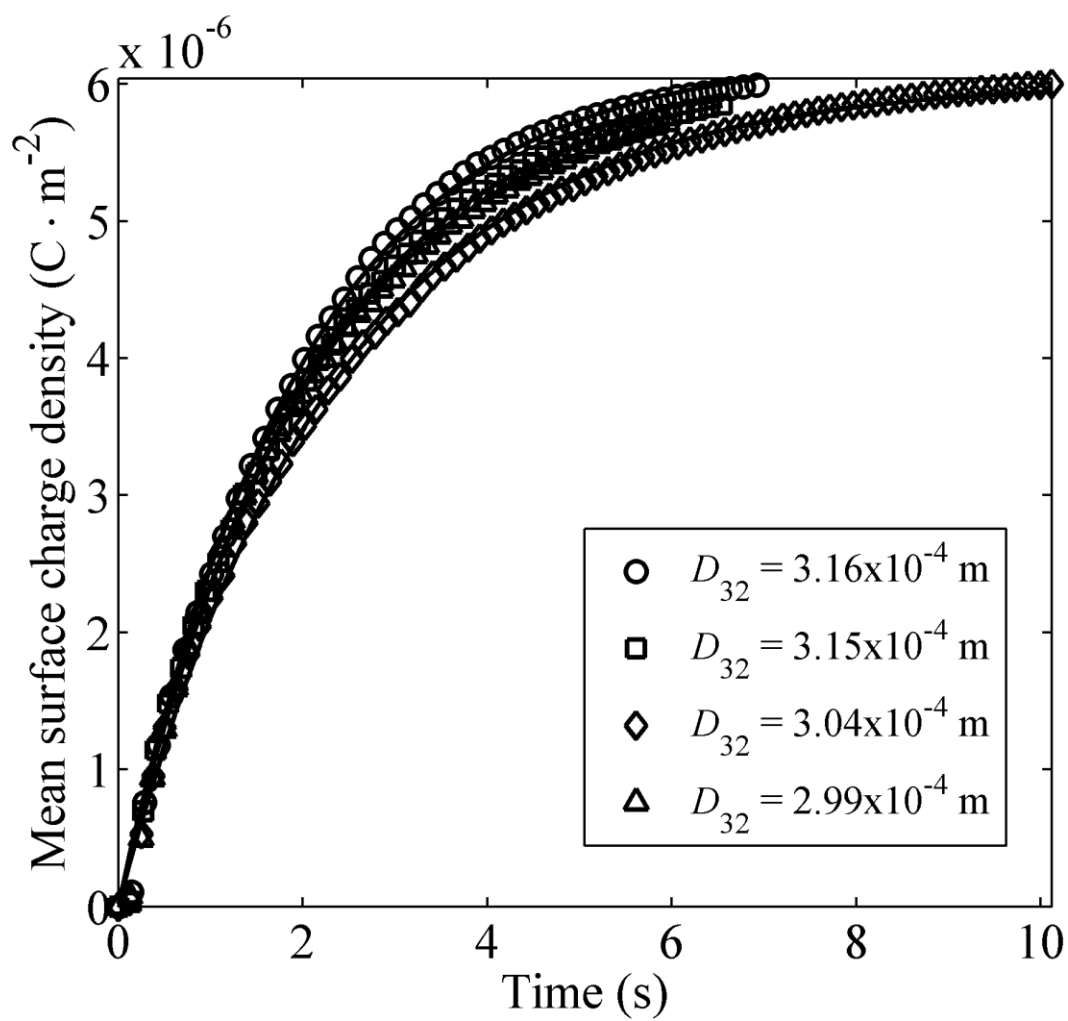
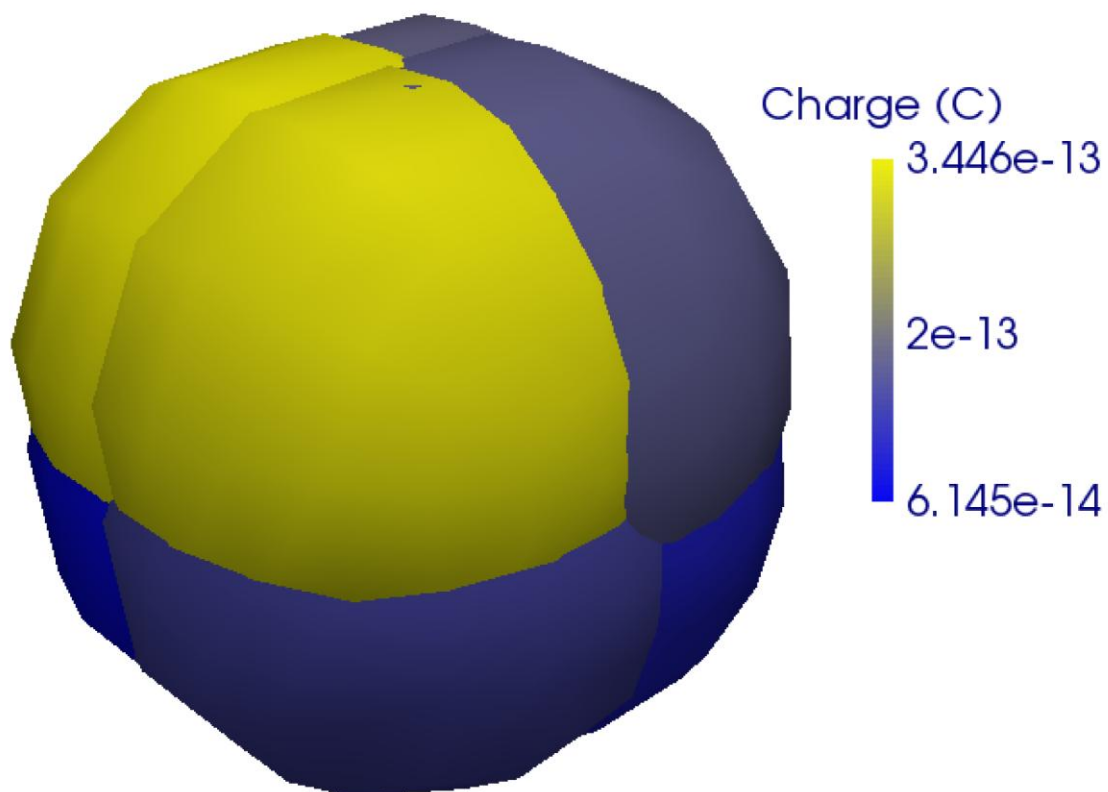
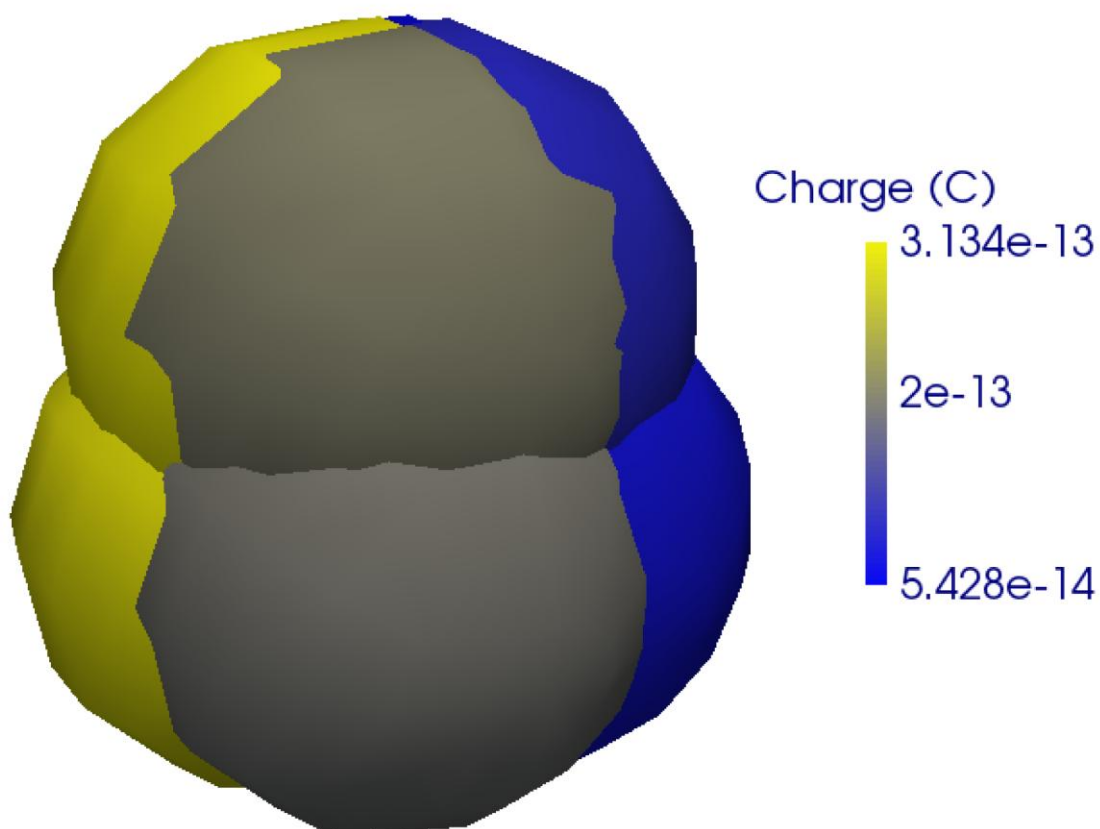


Fig. 16



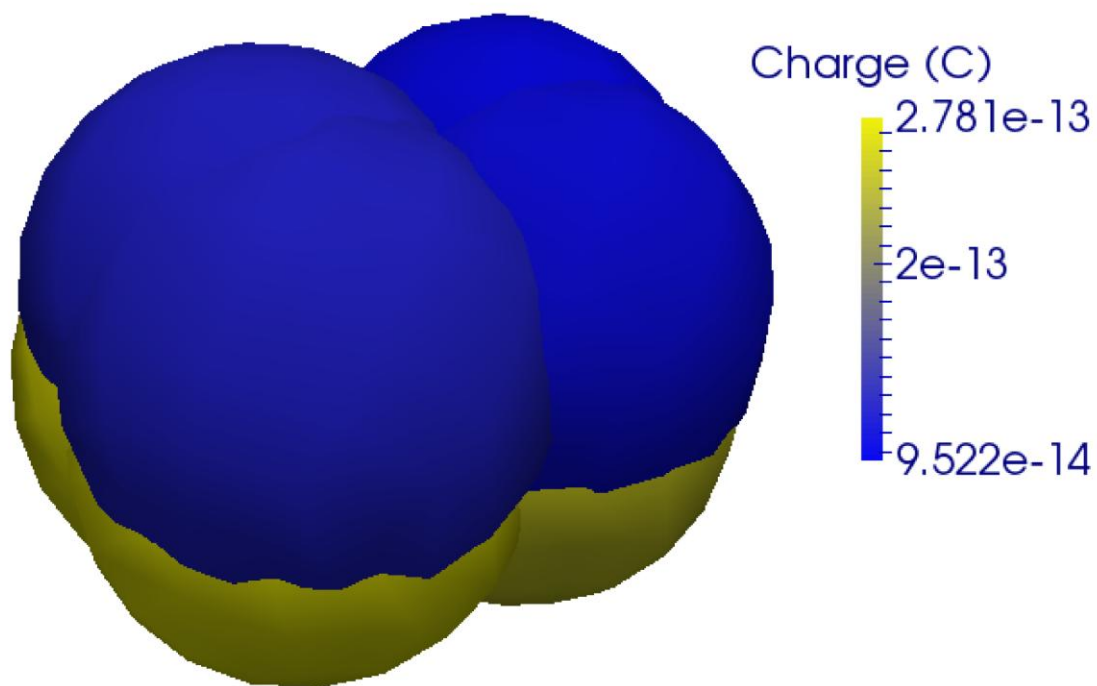
(a) Particle I ($D_{32} = 3.72 \times 10^{-4}$ m)

Fig. 17a



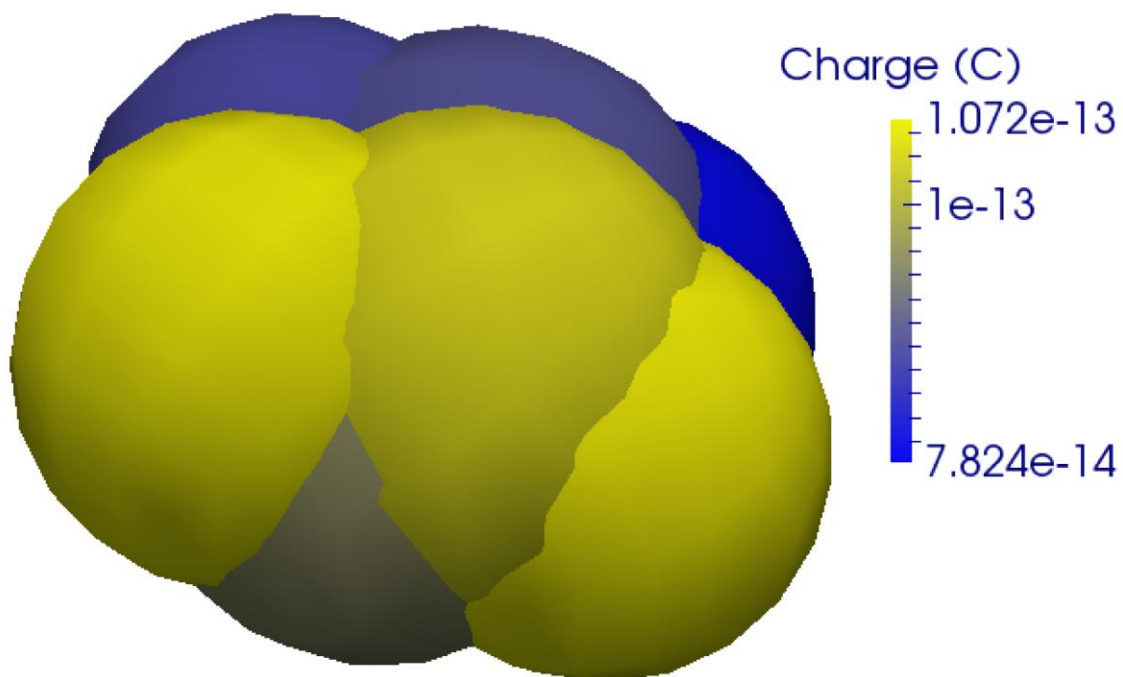
(b) Particle II ($D_{32} = 3.45 \times 10^{-4}$ m)

Fig. 17b



(c) Particle III ($D_{32} = 3.04 \times 10^{-4}$ m)

Fig. 17c



(d) Particle IV ($D_{32} = 2.71 \times 10^{-4}$ m)

Fig. 17d

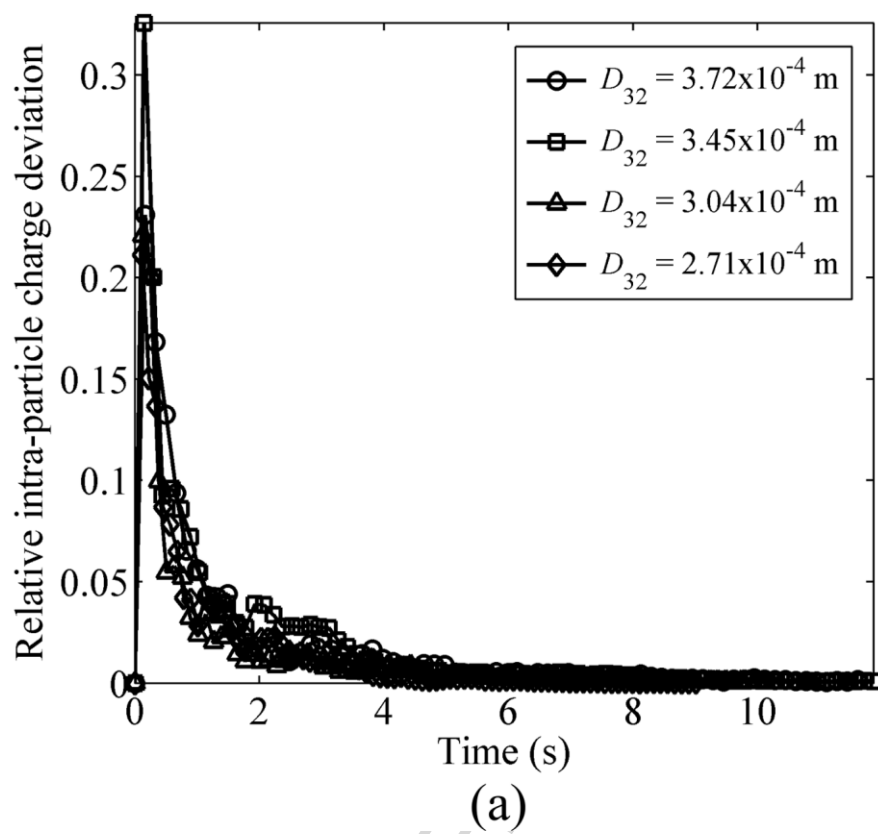


Fig. 18a

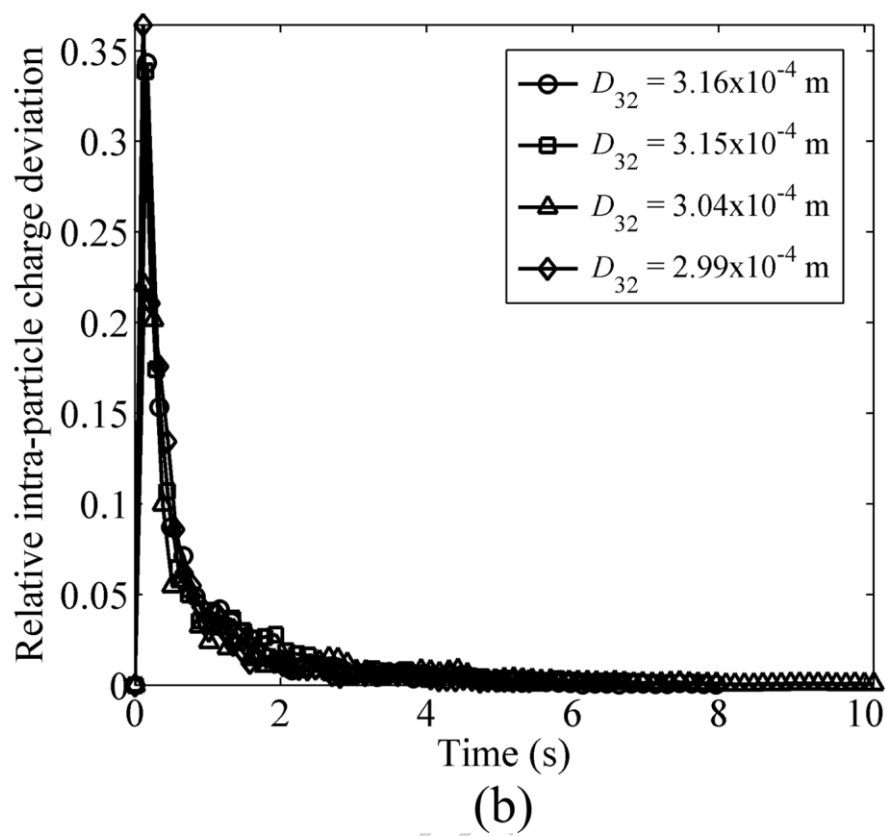


Fig. 18b

List of Tables

Table 1 Various particles with same D_{max} .

Table 2 Various particles with same D_v .

Table 3 Material parameters of the particle and the container.

Table 4 The shape factors and the charging coefficients for various particles.

Table 5 The charging coefficients of various particles with the same D_v .

ACCEPTED MANUSCRIPT

Table 1 Various particles with same D_{max} .

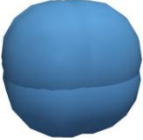
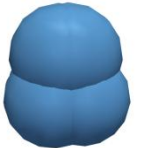
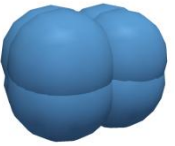
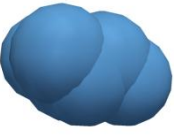
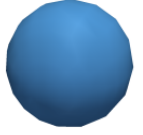
ID	Particle	D_{max} (m)	V_p (m ³)	A_p (m ²)	D_{32} (m)	ζ	Fill ratio
I		4×10^{-4}	2.79×10^{-11}	4.51×10^{-7}	3.72×10^{-4}	0.987	0.236
II		4×10^{-4}	2.38×10^{-11}	4.14×10^{-7}	3.45×10^{-4}	0.966	0.202
III		4×10^{-4}	1.84×10^{-11}	3.63×10^{-7}	3.04×10^{-4}	0.928	0.156
IV		4×10^{-4}	1.38×10^{-11}	3.04×10^{-7}	2.71×10^{-4}	0.913	0.117
V		4×10^{-4}	3.35×10^{-11}	5.03×10^{-7}	4.00×10^{-4}	1.0	0.284

Table 2 Various particles with same D_v .

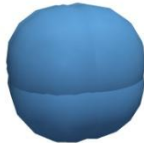
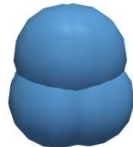
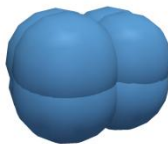
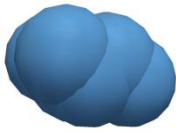
ID	Particle	D_v (m)	V_p (m ³)	A_p (m ²)	D_{32} (m)	D_{max} (m)	Fill ratio
I		3.27×10^{-4}	1.84×10^{-11}	3.41×10^{-7}	3.16×10^{-4}	3.48×10^{-4}	0.156
II		3.27×10^{-4}	1.84×10^{-11}	3.50×10^{-7}	3.15×10^{-4}	3.67×10^{-4}	0.156
III		3.27×10^{-4}	1.84×10^{-11}	3.63×10^{-7}	3.04×10^{-4}	4.00×10^{-4}	0.156
IV		3.27×10^{-4}	1.84×10^{-11}	3.68×10^{-7}	2.99×10^{-4}	4.40×10^{-4}	0.156

Table 3 Material parameters of the particle and the container.

	Particle	Container
Elastic modulus, Y (Pa)	8.7×10^9	2.1×10^{11}
Poisson's ratio, ν	0.3	0.3
Density, ρ ($\text{kg} \cdot \text{m}^{-3}$)	1.5×10^3	7.9×10^3

Table 4 The shape factors and the charging coefficients for various particles.

D_{32} (m)	ζ	k_c
3.72×10^{-4}	0.987	0.29
3.45×10^{-4}	0.966	0.36
3.04×10^{-4}	0.928	0.43
2.71×10^{-4}	0.913	0.54
Sphere(4.00×10^{-4})	1.0	1.28

Table 5 The charging coefficients of various particles with the same D_v .

ID	D_{32} (m)	k_c
I	3.16×10^{-4}	0.50
II	3.15×10^{-4}	0.48
III	3.04×10^{-4}	0.43
IV	2.99×10^{-4}	0.49

List of Figures

- Figure 1 The meshed particle with sample seeds on the surface.
- Figure 2 The multi-sphere generated with 500 primary spheres by the medial axis method.
- Figure 3 The multi-sphere generated with 10 primary spheres using merge optimization.
- Figure 4 The model setup of the rotating drum.
- Figure 5 The multi-spheres used in DEM simulation.
- Figure 6 The profiles of particle I ($D_{32} = 3.72 \times 10^{-4}$ m) during the drum rotation.
- Figure 7 The charge distribution for the particle I ($D_{32} = 3.72 \times 10^{-4}$ m) at $t = 0.33$ s.
- Figure 8 The charge evolution for the particle I ($D_{32} = 3.72 \times 10^{-4}$ m).
- Figure 9 The charge distributions in the drum with various particles at $t = 1.6$ s.
- Figure 10 An illustration of the polar coordinate.
- Figure 11 The evolution of charge density distribution ($C \cdot m^{-2}$) for the particle I ($D_{32} = 3.72 \times 10^{-4}$ m).
- Figure 12 The charge density distribution ($C \cdot m^{-2}$) of various particles at $t = 1.6$ s.
- Figure 13 The charge accumulation of various particles.
- Figure 14 The evolution of charge-to-mass ratio for various particles.
- Figure 15 The evolution of mean surface charge density for various particles.
- Figure 16 The evolution of mean surface charge density of various particles with the same D_v .
- Figure 17 Typical intra-particle charge distribution of various particles at $t = 1.66$ s.
- Figure 18 The relative intra-particle charge deviation of particles: (a) the same maximum diameter and (b) the same equivalent volume diameter.

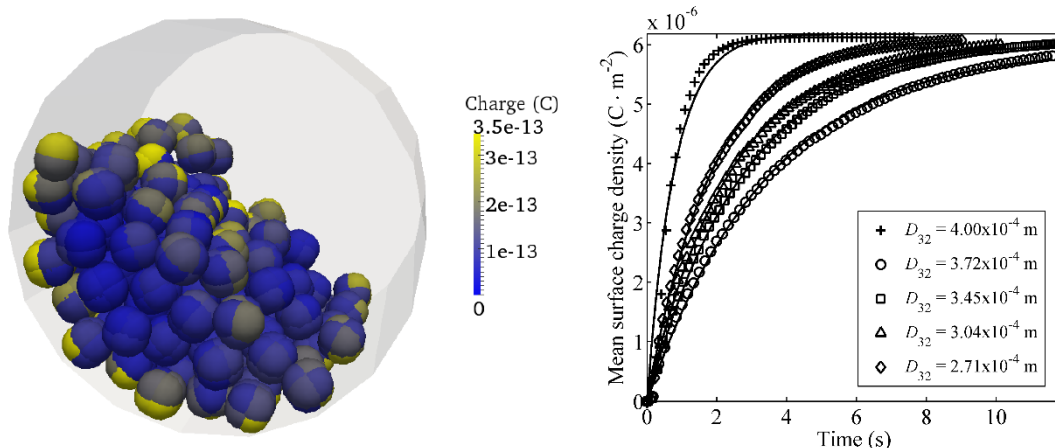
Numerical Analysis of Contact Electrification of Non-spherical Particles in a Rotating Drum

Chunlei Pei^{1,2,ζ}, Chuan-Yu Wu^{1*}, Michael Adams²

¹ Department of Chemical and Process Engineering, University of Surrey, Guildford, Surrey, GU2 7XH, UK

² School of Chemical Engineering, University of Birmingham, Birmingham, B15 2TT, UK

Graphical abstract



Typical charge distribution and accumulation of irregular particles.

^ζ Presently with Department of Materials Science and Metallurgy, University of Cambridge, Cambridge, CB3 0FS, UK

* Corresponding author: Tel: 01483683506. Email: c.y.wu@surrey.ac.uk

Numerical Analysis of Contact Electrification of Non-spherical Particles in a Rotating Drum

Chunlei Pei^{1,2,ζ}, Chuan-Yu Wu^{1*}, Michael Adams²

¹ Department of Chemical and Process Engineering, University of Surrey, Guildford, Surrey, GU2 7XH, UK

² School of Chemical Engineering, University of Birmingham, Birmingham, B15 2TT, UK

Highlights

- Contact electrification of irregular particles in a rotating drum is modelled.
- The irregular particle shape is modelled using a sphere-tree multi-sphere method.
- The charge gradually propagates from the near-wall region to the entire system.
- Non-uniform intra-particle charge distribution of multi-spheres is induced.

^ζ Presently with Department of Materials Science and Metallurgy, University of Cambridge, Cambridge, CB3 0FS, UK

* Corresponding author: Tel: 01483683506. Email: c.y.wu@surrey.ac.uk